Laser interferometry with gratings

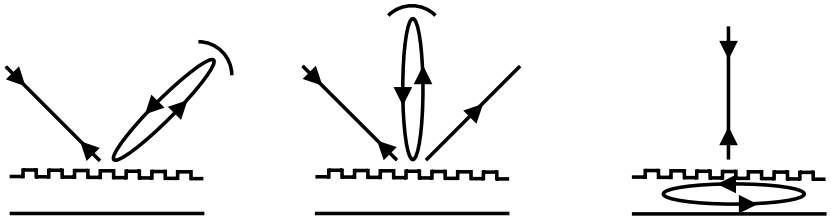

Von der Fakultät für Mathematik und Physik
der Gottfried Willhelm Leibniz Universität Hannover
zur Erlangung des Grades

Doktor der Naturwissenschaften
– Dr. rer. nat. –

genehmigte Dissertation von

Dipl.-Phys. Alexander Bunkowski,

geboren am 22. Februar 1976 in Kassel.

Dezember 2006

Referent:	JProf. R. Schnabel
Korreferent:	JProf. J. Arlt
Tag der Promotion:	20. Dezember 2006

Zusammenfassung

Der Einsatz von Interferometerkonzepten auf der Basis von verlustarmen Beugungsgittern soll die Empfindlichkeit zukünftiger Laserinterferometer zur Messung von Gravitationswellen steigern.

Im Rahmen dieser Arbeit wurde ein rein-reflektierender optischer Resonator mit einer Finesse von 1580 durch die Benutzung eines Reflexionsgitters in Littrow Anordnung erster Ordnung experimentell realisiert. Dadurch konnten bisher unerreichte Werte in Bezug auf hohe Beugungseffizienz (99,635 %) und niedrige optische Verluste (0,185 %) für ein dielektrisches Gitter nachgewiesen werden.

Erstmalig wurde die experimentelle Realisierung eines rein-reflektierenden Resonators durch die Benutzung eines Gitters in Littrow Anordnung zweiter Ordnung gezeigt. Im Gegensatz zu dem vorhergenannten Konzept, wurde dabei große Leistungsüberhöhung im Resonator durch den Einsatz eines Gitters mit niedriger (0,58 %) Beugungseffizienz erzielt.

Aufgrund der Geometrie des Resonatorkonzeptes interferieren drei, statt üblicherweise zwei Laserstrahlen gleichzeitig am Gitter, was zu neuen Resonatoreigenschaften führt. Eine theoretische Analyse von Phasenbeziehungen eines generischen Drei-Port Kopplers führte zur Erklärung dieser Eigenschaften und damit zu einer Verallgemeinerung der bisher bekannter Resonatortheorie. Die für die Resonatoreigenschaften verantwortlichen Phasen konnten als alleinige Funktion der Beugungseffizienzen dargestellt werden. Damit wurden Vorhersagen von Resonatoreigenschaften aufgrund von leicht zugänglichen Ergebnissen von Effizienzmessungen, bei völliger Unkenntnis des physikalischen Aufbaus des Gitters, möglich. Diese konnten im Experiment erfolgreich bestätigt werden.

Um dem Problem des thermischen Beschichtungsrauschens von hochreflektierenden Spiegeln entgegenzuwirken, wurde eine dünne, einlagige Beschichtung auf der Basis eines resonanten Gitterwellenleiters vorgeschlagen. Funktionsweise und Beispielrechnungen zum Design solcher Beschichtungen wurden vorgestellt.

Stichworte: Gravitationswellendetektor, Laserinterferometrie, Beugungsgitter

Abstract

The application of interferometric concepts on the basis of low-loss diffraction gratings should boost the sensitivity of future laser interferometers for the detection of gravitational waves.

In the context of this thesis an all-reflective optical resonator with a finesse of 1580 was experimentally demonstrated by using a reflection grating in a first order Littrow mount. Thereby, unprecedented values with respect to high diffraction efficiency (99.635 %) and low optical loss (0.185 %) for a dielectric grating could be verified.

For the first time the experimental realization of an all-reflective resonator employing a diffraction grating in a second order Littrow mount was shown. In contrast to the aforesaid concept, high power gain inside the resonator was achieved by employing a diffraction grating with low (0.58 %) diffraction efficiency.

Due to the geometry of the resonator concept, three – instead of the usual two – laser beams interfere at the grating simultaneously, leading to new resonator properties. A theoretical analysis of phase relations of a generic three-port coupler led to an explanation of these properties and thus, to a generalization of the previously known theory of resonators. The phases governing the properties of the resonator could be represented as functions which solely depend on diffraction efficiencies. Therefore, predictions about resonator properties could be made due to the easily accessible results of efficiency measurements; no knowledge about the physical properties of the grating was required. An experiment successfully validated these predictions.

To counteract the problem of coating thermal noise due to highly reflective mirrors, a thin, single layer coating on the basis of a resonant grating waveguide was proposed. Mode of operation and sample calculations considering the design of such gratings were presented.

Key words: Gravitational wave detector, laser interferometry, diffraction grating

Acknowledgements

Special thanks go to Oliver Burmeister and Daniel Friedrich. I hope they had as much fun working with me as I had working with them.

As a member of Roman's Advanced interferometry and squeezing light group I could not only enjoy our weekly group discussions and seminars, but I could also rely on many helping hands and minds. I am deeply grateful for the support I got from each member of the group.

A substantial part of my work resulted from a collaboration with the Institut für Angewandte Physik in Jena. I would like to thank Tina Clausnitzer, Stephan Fahr, Ernst-Bernhard Kley, and Andreas Tünnermann for working together with us and providing us with gratings.

I also want to thank Andreas Freise for the upgrade of his simulation software FINESSE in which I could participate. Some of our discussions were quite enlightening for me. For further interesting exchanges I want to thank Peter Beyersdorf from Stanford and San Jose State University who worked with us in the lab for one month and Roland Schilling with whom I had interesting conversations about phase relations.

Benno Willke, Gerhard Heinzel, and their respective GEO- and LISA-teams were a great resource of in-depth knowledge of interferometry, electronics, computers as well as many other things. Thank you for sharing!

I would also like to thank Jan Arlt from the Institut für Quantenoptik for being the second referee of my thesis and Paul Cochrane for proofreading.

With Roman Schnabel I was lucky to have a dedicated thesis advisor. He always took time to discuss our project. His scientific input as well as his humor and optimism showed me that it is possible to do science successfully and have fun at the same time.

At the Institut für Gravitationsphysik I found ideal conditions of work: A friendly atmosphere, motivated and skilled scientists, superb technical support, and enough funds to buy stuff and travel. I was guided when needed, but more importantly, I was given freedom to develop ideas. I would like to thank Karsten Danzmann for creating and leading such a place.

Contents

Chapter 1

Introduction

1.1 Historical notes on gravitational wave detectors and gratings

Almost 40 years ago Joseph Weber reported on coincidence measurements, conducted with aluminium cylinders at the University of Maryland and the Argonne National Laboratory, and concluded, that he found *good evidence that gravitational radiation has been discovered* [1.1]. Although his findings and subsequent claims [1.2–1.4] were never generally accepted by the scientific community, his work can retrospectively be considered a success, because he truly pioneered the field of experimental gravitational wave detection. Let's review briefly how the field evolved from being a venture of a single scientist (and his PhD-students) to multi-national efforts, which are operating the first generation of large-scale laser interferometers and are already heavily involved in researching novel techniques for second and third generation detectors. One of these techniques, namely the application of diffraction gratings as key optical elements in future interferometers, is the topic of this thesis. Hence, a short overview of the development of diffraction gratings will also be given.

The goal of gravitational wave detection is to sense distortions of space time that are triggered by accelerated masses and are travelling with the speed of light through space. Gravitational waves follow from Einstein's theory of General Relativity [1.5]. For a mathematically solid introduction to the topic see the classic text of Misner,

Thorne and Wheeler [1.6] or the newer, more descriptive approach by Schutz [1.7]. A passing gravitational wave will alter the distances between freely falling test masses with a characteristic frequency. In principle, gravitational wave detection consists of simple repetitive length measurements. It is the tininess of the relative length change $\Delta L/L$ to be detected which makes the task so extremely challenging. Although today's detectors can already measure strains $h = 2\Delta L/L$ that are smaller than 10^{-22} [1.8] the first generally accepted, direct detection of gravitational waves is yet to come.

1.1.1 Bar detectors

Weber employed cylindrical aluminium bars for the length measurement. It was thought that a gravitational wave could excite a resonant mode of the bar and the movement would be transformed into a recordable voltage by an attached piezoelectric transducer. His measurement principle is still used in today's resonant bar and sphere detectors such as AURIGA [1.9], EXPLORER [1.10], NAUTILUS [1.10], Mario Schenberg [1.11], and MiniGRAIL [1.12]. Most of these detectors evolved from group efforts that tried to reproduce or falsify Weber's claims [1.13–1.17]. These efforts were necessary because the signals he claimed to have measured were far too strong to fit into the generally accepted theory. Hence, a reproduction of his results would have been a twofold sensation: a confirmation of the first direct detection of gravitational radiation and a proof that existing theories were wrong or incomplete.

The race for more and more sensitive detectors was opened. Several groups around the world began to construct bar detectors and develop new techniques to boost their sensitivity. However, even detectors that were far more sensitive than Weber's could not reproduce his results. The expected weak signals in gravitational wave detectors are buried in noise from many different sources. From today's point of view one could say that Weber's inadequate use of statistics in his data analysis was responsible for his false claims. He simply misinterpreted noise as gravitational wave signals.

The falsification of Weber's results did not stop the race for more sensitivity. The scientific community of bar detectors had been established. Though knowing that they were orders of magnitude away from the sensitivity needed for a detection, their members have been pushing technology and their detectors ever since. However, due to their limited measurement bandwidth they are somewhat in the shadow of the

kilometer-scale laser-interferometric detectors that have come online over recent years.

1.1.2 Laser interferometers

Interferometric gravitational wave detectors employ light to sense the distance between suspended mirrors, the so-called test masses. The idea was first published by two Russians, M. Gerstenshtein and V. I. Pustovoit, in 1962 [1.18]. According to Harry Collins [1.19], Weber and his students independently considered this idea in 1964. Several years later the first interferometric detector [1.20, 1.21] on the basis of a Michelson interferometer was built in Malibu, California by Robert Forward a former coworker of Weber. Forward realized that the response of interferometric detectors is not constrained to a narrow frequency band as it is the case for the bar detectors. Hence, the vision of a wideband gravity antenna acting like an astrophysical telescope was born.

In 1972 Rainer Weiss from MIT in Cambridge, Massachusetts was the first to systematically analyze the potential sources of noise that would limit the performance of a gravitational wave detector [1.22]. With this work he laid the foundation for subsequent prototypes and large scale detectors. Around 1975 a German group at the Max Planck Institute for Astrophysics in Munich entered the game of interferometry by first developing a three meter instrument and later a very successful 30 meter prototype. The first prototype interferometer in Glasgow, Scotland was built by Ronald Drever in 1976. Caltech in Pasadena, California joined the interferometry effort by hiring Drever to develop a 40 meter prototype in 1979.

Simultaneous to the prototyping work, plans for kilometer scale interferometers, sensitive to gravitational waves in the range from 10 to 10^3 Hz, were made. In a collaborative effort, the MIT and Caltech groups received funds to build the Laser Interferometer Gravitational Wave Observatory, (LIGO) [1.24]. With two 4 km and one 2 km interferometers at two sites, Hanford, Washington and Livingston, Louisiana, it is the biggest and most influential project. Many of the data analysis and research and development activities in the field are conducted within the LIGO Scientific Collaboration (LSC) [1.25] by its more than 500 individual members [1.26].

In Europe, an Italian-French collaboration was formed to build a 3 km detector, called VIRGO [1.27], near Pisa, Italy. The Glasgow and Munich group also planned to build a 3 km instrument [1.28] in the Harz mountains, Germany. But funding

difficulties led to the construction of the smaller GEO interferometer [1.29] near Hannover, Germany. With the shorter arm length of 600 meters it relies on advanced techniques [1.30, 1.31] to compete with the bigger projects. Moreover, there is the Japanese project TAMA [1.32] with a 300 meter interferometer near Tokyo.

After around ten years of construction and commissioning work, the LIGO- and GEO- detectors have approached their design sensitivity. At the time being they jointly participate in the long term data-taking run S5. The VIRGO detector is still being commissioned [1.33] and will start to take data later.

There are already plans for the future of current detectors. After S5, LIGO will get some technical upgrades and by around 2011–2014 the Advanced LIGO detector [1.34] is to be installed. This so-called second-generation detector is expected to have a ten-fold increase in sensitivity. Similar upgrades are planned for VIRGO [1.35]. GEO will be upgraded to a high frequency detector GEO-HF [1.36] and will continue to serve as a test bed for novel interferometer techniques. Moreover there is an Australian consortium planning to build a detector [1.37] and the Japanese TAMA-team is suggesting a cryogenic interferometer [1.38].

The development of detectors will not stop with its second generation. The short-term goal of current- and second-generation detectors is certainly the first direct detection of gravitational waves. But there is also a long-term goal, which is the creation of a new kind of astronomy. Once interferometers are sensitive enough to detect signals on a regular basis a *new window onto the universe* [1.39] will be opened. Whereas traditional astronomy primarily relies on the observation of some part of the electromagnetic spectrum, gravitational wave astronomy will have the unique opportunity to access sources which do not emit electromagnetic radiation and to access times when the universe was not transparent to such radiation.

Besides the future space-based LISA interferometer [1.40], which is designed to measure gravitational waves in a complementary frequency range of 10^{-4} to 10^{-1} Hz, there will also be third-generation ground-based detectors with increased sensitivity. Concepts for third-generation detectors have been developed in the past and are being developed now. Such detectors will be critical in almost all its constituents. Hence, research is carried out in a variety of fields such as high-power laser stabilization, feedback control systems, pendulum suspension systems, squeezed light states, cryogenic

interferometers, optical coatings, material sciences and more. Third generation detectors will emerge from a tradeoff between desired frequency response, available funds and some of the newly developed technologies.

One of these new technologies is the use of diffractive optics. In 1995 Drever already proposed to use diffraction gratings as all-reflective beam splitters in laser interferometers instead of partly transmitting optical components [1.41]. Thereby all sensitivity limiting effects that are associated with absorbed power in optical substrates would be avoided. Robert Byer's group at Stanford University, California took up the idea and experimentally realized some all-reflective interferometer topologies [1.42] on the basis of commercially available diffraction gratings [1.43].

However, the optical properties and quality of commercially available gratings did by no means meet the requirements for high precision interferometers, especially those for gravitational wave detection. Hence, in 2003 a project was started to investigate interferometers on the basis of diffraction gratings that were especially designed and manufactured for this purpose. Two areas of expertise, namely microstructure technology at the Institut für Angewandte Physik in Jena and laser interferometry at the Institut für Gravitationsphysik in Hannover were brought together in a Collaborative Research Center of the Deutsche Forschungsgemeinschaft. The results reported in this thesis were accumulated within this project.

There was a second research effort at the University of Florida aimed at using diffraction gratings to enhance the sensitivity of interferometers. It was thought that pairs of gratings in the interferometer arms could form *white light resonators* [1.44]. The reader should note that our approach is not based on this temporarily misunderstood concept [1.45, 1.46].

1.1.3 Diffraction gratings

Elements that show a periodic modulation of their optical properties are termed gratings. For more than two decades scientist have used them intensively for various applications, and in the middle of the last century it was even said, that *"No single tool has contributed more to the progress of modern physics than the diffraction grating, especially in its reflecting form"* [1.47]. The importance of diffraction gratings was mainly due to their ability to disperse light in its constituent spectrum; thereby

enabling many spectroscopic discoveries.

The classic diffraction grating consists of a one dimensional corrugation, the so-called grating grooves, of a surface with a fixed period. The period is usually of the order of the light's wavelength. Traditionally, ruling machines were used to manufacture such small structures by employing a sharp diamond tip to scratch parallel lines into a soft metal.

In the late 60s of last century an alternative production method was demonstrated [1.48] which was based on a lithographic process. A stable interference pattern of two laser beams is recorded in photoresist and, after wet development, becomes the grating lines. Chemical etching can then be used to transfer the grating into the substrate. This method is much faster than ruling, because the whole grating area is exposed simultaneously. However, the generation of a uniform interference pattern of large size is challenging, because it requires a plane wavefront of the laser beams over the whole grating area. Another problem is the control of the groove profile, which is usually restricted to have sinusoidal form. Despite these difficulties, recent development of lithographic interference technology (also termed holographic method) led to large area, high diffraction efficiency gratings of impressive size and quality that are, for example, to be used as pulse compressor/stretcher in Petawatt laser systems [1.49].

Instead of using an interference fringe to generate the grating pattern one can also use a single, strongly focused beam to directly write the grating structure into the resist, a technique that is well known from microelectronic chip production. While not as fast as the lithographic interference approach, direct writing has a very high resolution due to the short wavelength and the strong focus of the laser beam or the ion beam used for writing. Modern microstructure technology allows for many different kinds of diffractive optical elements with varying periods, curved grooves, and varying groove shapes for manifold optical functionalities, which include beam shaping, waveguide coupling, spectral filtering and many more [1.50]. Nowadays the term grating refers also to some of these more complex structured diffractive optical elements.

The gratings discussed in this thesis are all one-dimensional with a single period and rectangular groove patterns that were produced by ion beam direct writing. They were either etched into an optical substrate or into a layer of a dielectric coating.

1.2 Current and future interferometers

To understand the potential application areas of diffraction gratings in future gravitational wave interferometers, it is worth examining several aspects of today's detectors. Although third-generation detectors may differ considerably in terms of size and technology, they will encounter similar noise sources limiting their performance. The use of gratings could overcome some of these. While all-reflective optics avoids all noise issues associated with absorbed laser power in optical substrates and will give access to better test mass materials, grating waveguide coatings have great potential to reduce coating thermal noise.

1.2.1 Optical configurations of interferometric detectors

All current large-scale detectors [1.24, 1.27, 1.29, 1.32] are based on Michelson laser interferometers, which measure the phase difference of two light fields that have propagated up and down two perpendicular arms, see Fig. 1.1. The optimal arm length of

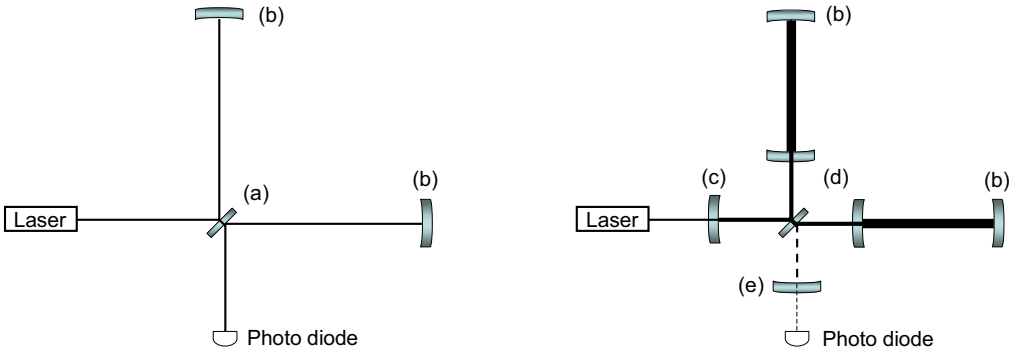

Figure 1.1: (left) A Simple Michelson interferometer with (a) a central partly transmissive mirror acting as a 50/50 beam splitter and (b) two highly reflective end mirrors; (right) Additional partly transmissive mirrors form cavities to (c) increase power inside interferometer, (d) store light in interferometer arms, and (e) enhance gravitational wave induced sidebands.

a simple Michelson interferometer for detecting gravitational waves is given if the light travel time in the arms is equal to half a gravitational wave period. This corresponds to a length of 750 km for a gravitational wave with a frequency of 100 Hz; a length

that is highly impractical to achieve if one considers that the interferometer must be housed in a vacuum system.

Advanced versions of the Michelson interferometer allow one to increase the interaction time of the light with the gravitational wave while keeping the physical length of the arms manageable. Herriott Delay lines [1.51] and Fabry-Perot resonators are two techniques used to increase the travel time of the light in the arms. The techniques of Signal Recycling [1.52] or Resonant Sideband Extraction [1.53] rely on enhancing the gravitational wave induced sidebands. Power Recycling is used to increase the overall circulating laser power inside the interferometer, thereby decreasing the shot noise of the laser light, which can limit the sensitivity of the observation band at high frequencies.

Except for delay lines, which are only used in GEO600, all above mentioned techniques are based on optical resonators. These are formed by adding partially transmissive mirrors to the optical path of a simple Michelson interferometer, as shown in Figure 1.1. As a consequence, the complexity of the interferometer – and the difficulties to control it – grows considerably. Moreover, the quality requirements of the optical components are much higher in complex interferometer configuration than in simple ones. This is especially the case in interferometers with nested high-finesse cavities as they are extremely susceptible to optical losses.

First generation detectors use a combination of some of the above mentioned advanced techniques. The LIGO and VIRGO detectors both use Power Recycling and arm resonators, whereas a combination of Power- and Signal Recycling, called Dual Recycling [1.31], is used in GEO600. Advanced LIGO, the only second generation detector that is in a mature planning phase, will use all three advanced resonator concepts as shown in Figure 1.1.

What about third-generation detectors, which will probably be installed between the years 2015–2020? They have not yet been designed. Their optical configuration will depend on the research and development that is carried out now, and might be based on a Sagnac- instead of a Michelson configuration [1.54] or other advanced quantum-non-demolition configurations [1.55]. Most likely, they will also make use of injected squeezed light states, a technique which was proposed more than 20 years ago [1.56], and has just recently matured far enough to be considered for implementation in a

detector [1.57], and would also have an effect on the optical layout of the interferometer. At the time being it seems to be too early to speculate about the specific design. But independent of the finally chosen combination of optical techniques, third-generation detectors will certainly employ optical beam splitters with various splitting ratios. Their coatings and the fact that they are used in transmission can lead to sensitivity limitations. Let's see what kind of optical properties these beam splitters should show and how these properties are conventionally achieved.

1.2.2 Key optical components

The mirrors shown in Fig. 1.1 act differently on the laser light. The ratio of reflected to transmitted light is about 1 for the central mirror (a), around 10^5 for the end mirrors (b), and, depending on the desired finesse, between 10 and 10^3 for the resonator couplers (c,d,e). The desired reflectance is achieved by means of dielectric multilayer coatings [1.58], with an overall thickness of several microns. To minimize multiple reflections at the two surfaces, usually one side of the mirror has an anti-reflective coating.

Although acting quite differently, the mirrors share a common feature: they always split an incoming beam into one reflected and one transmitted beam. This means, viewed functionally, one input leads to two outputs. Considering both output ports as two possible input ports, every beam splitter is a device with four ports. In the case of normal incidence, incoming and reflected beams counter propagate and hence two ports are pairwise degenerate. As we will see later, these apparently obvious features do not necessarily hold for grating beam splitters.

The mirror substrates are cylindrical with their circular surfaces coated. For current detectors the surfaces are either flat or spherical to support a Gaussian mode within the interferometer. Differently shaped surfaces to support so-called Mesa modes are also currently being discussed [1.59]. With a diameter of 15–25 cm and a thickness of around 10 cm the substrates weigh around 5–12 kg [1.60]. Future detectors will utilize even heavier mirrors to compensate for the increased radiation pressure noise which accompanies higher laser power. For Advanced LIGO the weight will already be 40 kg. One should note that high (e.g. currently $\sim$ 2 kW for GEO's central beam splitter) circulating laser power is sent *through* some of these thick substrates.

Optical loss inside the interferometer reduces its build-up power and hence the sensitivity. Therefore, only extremely low loss components can be used. Optical loss is mainly due to absorbtion of light in the substrate and in the coating, as well as scattering at the surfaces. Hence coating and substrate materials must be made of highly transparent materials [1.61] and the surface must be polishable to extreme surface flatness [1.62]. Again, the situation changes when gratings are considered; the surfaces are deliberately corrugated to make use of diffracted orders which can be considered as directed scattering. Furthermore, opaque materials with favorable mechanical and thermal properties can be used as substrates for all-reflective interferometers.

These thermal and mechanical properties of test masses are of uttermost importance, because the sensitivity limit of an interferometer not only depends on the *ability to measure the difference in phase of the returning light* from the interferometer but also on *extraneous forces on the test mass which mask the gravitational wave strain* [1.67]. Hence, not only are the previously mentioned optical techniques crucial to the detector but also the materials and techniques used to limit extraneous forces known as thermal-, seismic- and gravity-gradient noise.

Seismic noise refers to all motions induced by mechanical coupling to the environment. Isolation is provided by suspending the mirrors as multistage pendulums with a resonance frequency below the gravitational wave band. It is anticipated that current technology will allow suppression of seismic noise to a negligible level for the whole detection band of third-generation detectors [1.67]. Gravity-gradient [1.68] noise is due to time-dependent distribution of masses around the detector and will create a low-frequency observation limit at roughly 10 Hz for future ground based-interferometers. Thermal noise seems to be the most problematic extraneous force and will therefore be discussed in the next section.

1.2.3 Thermal noise

All thermally induced movements or distortions of the test masses which potentially limit the sensitivity of a detector can be classified as thermal noise. They include firstly, motions of the substrate surface due to mechanical loss in the test masses or the suspension, which can mask gravitational waves and secondly, perturbations to the substrates due to absorbed laser power preventing the detector to operate properly.

Let's start with the latter.

Absorbed laser power in a transmitted substrate and its coatings causes a temperature gradient within the test mass which is on the one hand responsible for a deformation of the surface due to a nonzero thermal expansion coefficient α, and on the other hand forms a thermal lens due to the temperature dependence of the refractive index $\beta = \mathrm{d}n/\mathrm{d}T$ [1.63]. As a consequence, the wavefront of the laser light will be distorted which can lead to unstable operating conditions of the interferometer [1.64, 1.65]. Thermal lensing will already be a problem for Advanced LIGO and needs to be compensated [1.66]. For more advanced detectors these effects can set a limit on the circulating laser power and hence on the shot noise limited sensitivity. High thermal conductivity, low optical absorption, as well as low values for α and β are favorable properties of transmissive test mass materials to minimize thermal lensing and deformation.

As indicated above, mechanical losses of the test masses and suspensions are also closely associated with thermal noise. For a mechanical system increasing the Q-value – i.e. decreasing mechanical loss – is accompanied by more thermally induced motion at the resonance frequency but with less motion away from the resonance. The common strategy to minimize thermally induced motions in the measurement band is to gather the thermal energy into narrow resonances of high-Q materials. The resonance frequencies are either out of band (*below* for the fundamental modes of the suspensions, *above* in the case of test mass resonances) or in-band (in the case of suspension fibre resonances), but occupying a negligible span in frequency. Hence, high-Q materials ought to be used for substrates to minimize *inner thermal noise* [1.69]. Another thermal noise source given through local deformations of the substrate surface, is *thermoelastic noise* [1.70, 1.71] which depends on several other material parameters such as specific heat, Young's modulus, Poisson ratio, and thermal expansion coefficient.

Moreover, recent studies have shown that the contribution of the high reflectivity mirror coatings to thermal noise is larger than previously thought [1.72]. With demonstrated coating technology the sensitivity for the planned Advanced LIGO detector would be dominated by coating thermal noise in a substantial part of the measurement band. Hence, finding ways of achieving high reflectivity without compromising the low thermal noise requirements is an urgent challenge for the development of future

detectors. One approach is to use thin single layer grating waveguide coatings as is proposed in this thesis.

Another method to reduce thermally driven motions, since they are proportional to temperature, is to cool test masses and suspensions. A Japanese group is successfully prototyping this approach [1.73]. For this technology one important issue will be the heat input to the test masses from the laser. Again, extremely low power absorption and high thermal conductivity for effective cooling is an essential premise for the test mass material. In addition, the change of material properties for cryogenic temperatures has to be considered.

Taking into account all the above requirements, fused silica and sapphire seem to be the only adequate candidates for transmissive test masses in connection with the currently used Nd:YAG laser wavelength of 1064 nm. Fused silica is used in all first generation detectors and will be used in Advanced LIGO. However, due to increased mechanical loss at low temperatures and relatively low thermal heat conductivity, fused silica is an unfavorable material for cryogenic interferometers, where sapphire is better suited [1.74].

One major constraint in choosing an appropriate test mass material is the requirement of high transparency for the optical wavelength being used. Using non-transmissive optical elements (all-reflective interferometer topologies) allows for a wider choice of materials. Opaque for 1064 nm light, silicon is a high-Q material with outstanding thermal and mechanical properties which may allow for a reduction of thermal issues in future interferometers [1.75].

High thermal conductivity paired with low thermal expansion would minimize thermal deformation of substrates and hence allow for more power inside the interferometer as compared to fused silica or sapphire [1.76]. Additionally, silicon has a vanishing thermal expansion coefficient for certain low temperatures which indicates the possibility of vanishing thermo-elastic noise for cryogenic detectors operating at these temperatures [1.75].

After this short overview of first-, second- and possible third-generation laser-interferometric gravitational wave detectors as well as their optical technologies and noise limitations, the next section will briefly summarize the reasons for using gratings in future detectors.

1.2.4 Advantages of grating interferometers

Third-generation earth-bound gravitational wave detectors will most likely be limited by various thermal noise sources in the intermediate frequency band (between around 10 Hz and several 100 Hz) and shot noise in the high frequency band (above several 100 Hz). To beat this noise floor, new optical technologies and materials are being researched and developed. Using diffraction gratings is promising due to their multiple benefits:

- All-reflective interferometer topologies avoid *all* thermal issues that are associated with absorbed laser power in transmitted optical substrates, thereby allowing for more light power and hence a reduced shot noise level.
- Additionally, they permit opaque test mass materials, e.g. silicon, with superior thermo-mechanical properties. Silicon has the potential to reduce thermal noise in mid-frequency cryogenic detectors as well as in high-frequency room-temperature detectors [1.77].
- Thin single-layer grating waveguide coatings may reduce coating thermal noise in the intermediate frequency band.

However, the fields of all-reflective interferometry and grating waveguide coatings are relatively new and hence not as mature as other technologies. While some basic concepts have been proposed and realized in proof of principle experiments, others have not been experimentally demonstrated prior to this work. The next section gives an overview.

1.3 Interferometry concepts based on gratings

Diffraction gratings are traditionally used in connection with polychromatic light for their dispersive characteristics in devices such as spectrographs, optical pulse compressors, wavelength division multiplexing systems, and many others, see e.g. Reference [1.78]. By contrast, laser-interferometric applications are for essentially monochromatic light, where either single gratings can serve as high reflectance mirrors, or in combination with multilayer coatings, serve as all-reflective beam splitters.

1.3.1 All-reflective interferometers

A surface with a periodic modulation of optical properties, so-called grooves, defines a diffraction grating. Let's have a look at Figure 1.2 and consider incident light of wavelength λ in the plane perpendicular to the grating grooves and its surface. For a

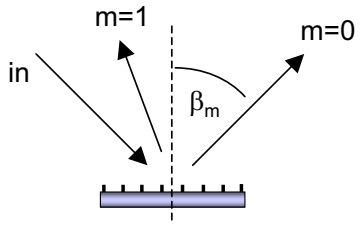

Figure 1.2: A grating illuminated by a beam (in). The number of outgoing beams are given by the grating equation (1.1). The beams are numbered by an integer (m) and the angles with respect to the grating normal are given as β_m. The angle of the incident light is $\alpha = -\beta_0$. Shown is a non-Littrow mount. See Reference [1.78] for different sign convention of the angles.

grating period d and an incidence angle of α, measured from the grating normal, the angle β_m of the mth diffraction order is given by the well-known grating equation

$$\sin\alpha + \sin\beta_m = m\lambda/d. \tag{1.1}$$

Note, that Equation (1.1) only predicts the number and angles of diffraction orders but not the distribution of power between them. For a short introduction to grating efficiency calculations, see Appendix A.

For transparent materials the orders will exist in transmission and reflection. One obtains an all-reflective beam splitter when the grating is combined with a high reflectivity coating, or transmitted orders are suppressed by some other means. The zeroth order of such a splitter represents specular reflection and is always present in contrast to the higher orders. The existence of higher orders depends on the choice of d and α. For our purposes only one or two additional orders are required, so that $d \sim \lambda$.

For appropriately chosen parameters there is only one additional diffraction order and no degeneracy of ports ($\alpha \neq \beta_1$), thus one obtains the analog to a four-port mirror as introduced in Section 1.2.2. This device enables, for instance, an all-reflective version of a Michelson interferometer as shown in Figure 1.3, provided that the efficiency for

the specular reflection and for the diffraction into the first order are roughly the same.

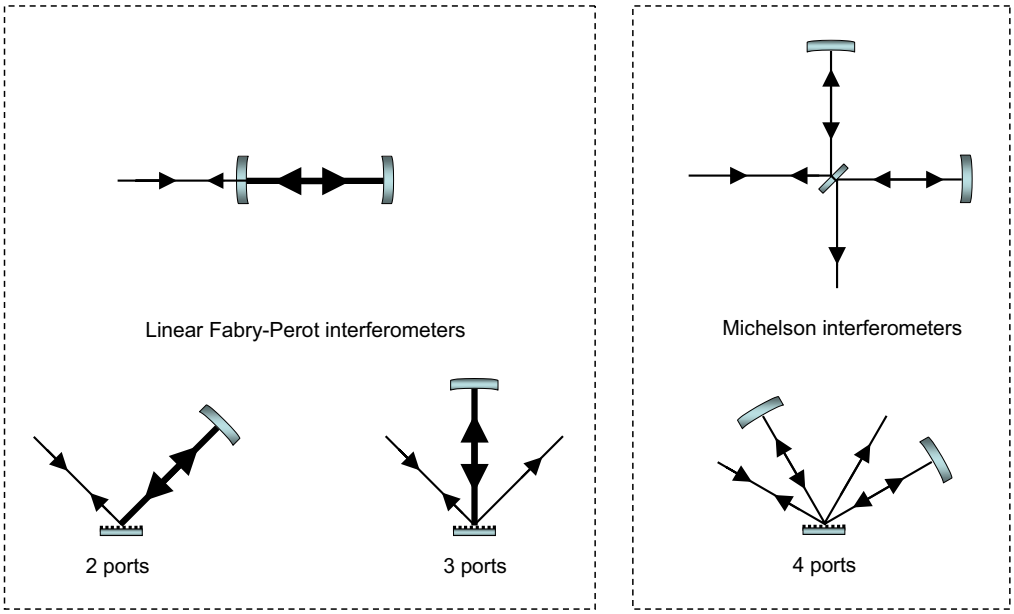

Figure 1.3: (top) Sketch of a Michelson and a linear Fabry-Perot interferometer with transmissive optical elements and (bottom) possible all-reflective realizations of these devices based on diffraction gratings. Note that the Fabry-Perot interferometer can either be realized with a grating in first-order (resulting in two ports) or second order Littrow mount (three ports).

The analog to a transmissive mirror with two ports (in the case of normal incidence) is given for a first order Littrow configuration ($\alpha = \beta_1$). In this case an all-reflective linear Fabry-Perot interferometer can be constructed, also shown in Figure 1.3. The maximal finesse of such a cavity is limited by the first order diffraction efficiency of the grating that is used to couple light to the cavity.

Parameters can likewise be chosen to allow for a second order Littrow configuration ($\alpha = \beta_2$), which results in a beam splitter with 3 ports, which can also be used to construct a linear Fabry-Perot interferometer (Figure 1.3). Its maximal finesse is limited by the specular reflectivity of the grating rather than its diffraction efficiency. However, such a 3-port splitter has no simple analog to a conventional transmissive mirror.

In the first published proposal [1.41, 1.79] which put forward the idea of using diffractive elements to split beams in interferometric gravitational wave detectors, Ron Drever argued that concepts relying on low diffraction efficiency gratings were favorable. The idea was, that mirrors with a weak periodic perturbation for low diffraction efficiency ($\sim$ 1 %) would show less optical loss than gratings with high diffraction efficiency. Consequently, complex interferometer topologies (including recycling techniques), that are based solely on low diffraction efficiency gratings to split beams were proposed.

However, experimental realizations [1.42] of all-reflective interferometers just included a 50/50 grating beam splitter to build a Michelson and Sagnac interferometer as well as a high diffraction efficiency grating to build a cavity in first order Littrow mount [1.81]. The metal grating used for the all-reflective Michelson interferometer showed high optical loss of about 3.6 %, the one used for the Fabry-Perot interferometer had a diffraction efficiency of only 91 % allowing for a cavity with a modest finesse of 53.

Although the initial experiments were important in the sense that they proved some of the previously proposed concepts, they did not demonstrate the favorable topology of a linear cavity coupled by a low diffraction efficiency grating, nor did they show that grating quality is anywhere close to that required for gravitational wave interferometers. Our project aimed at demonstrating and understanding the previously proposed but up to then unrealized concept as well as improving the quality of gratings. In the focus of this thesis are the cavity concepts with gratings in first and second order Littrow mount. Two other theses [1.82, 1.83] within our project are concerned with all-reflective Michelson interferometers.

1.3.2 Grating waveguide coatings

In the all-reflective interferometer concepts introduced in the last section, the high reflectance of the gratings is usually achieved by means of a multilayer coating. However, a grating in combination with a single horizontal layer can also provide high reflectivity.

When a periodic structure is used to couple light diffractively into a waveguide, the resulting device can show reflection peaks for a certain wavelength and incident angle.

It has been noted by several authors (see e.g. [1.84, 1.85]) that such grating waveguide structures (GWS), can exhibit a theoretical peak reflectivity of 100 %. Unlike conventional high reflectance devices which are based on multiple interference between many layers with different refractive indices, a GWS can provide perfect reflectivity using just a single layer.

With this remarkable property in mind I propose a high reflectivity coating based on a GWS, and show that if the GWS design is simultaneously optimized for a thin waveguide layer and a broad reflection peak, such a coating can serve as a low thermal noise alternative to a conventional multilayer coating.

1.4 Structure of the thesis

In the following main chapters of this thesis, six peer reviewed articles that have been written in the context of this project are presented. They are ordered with regards to their content rather than their chronological date of issue as explained below.

Chapter 2 takes up the previously demonstrated cavity concept on the basis of a grating in first order Littrow configuration. It is shown that careful custom design and fabrication of a grating can lead to unprecedented high diffraction efficiency resulting in the experimental demonstration of a high finesse cavity, for this previously assumed unfavorable design.

The Chapters 3 through 6 form a unit because they are all concerned with three port interferometry. The first experimental realization of a three-port coupled cavity in second order Littrow configuration is reported in Chapter 3. Due to the additional port this cavity exhibits features not present in conventionally coupled resonators. These new features are theoretically analyzed and explained in Chapter 4. By tuning certain properties in the production process of gratings it is shown experimentally in Chapter 5, that the predicted new features can be successfully controlled. The final activity committed to three port interferometry is reported in Chapter 6, where a generalization of the theoretical consideration of Chapter 4 is performed.

A proposal of a high reflectivity but low thermal noise coating on the basis of a grating waveguide structure is reported in Chapter 7.

Chapter 8 provides some overall conclusions and an outlook for further research

directions towards future laser interferometric detectors employing gratings. The appendices provide some additional information that were not published in the journal articles.

References

[1.1] J. Weber, *Evidence for the Discovery of Gravitational Radiation,* Phys. Rev. Lett. **22**, 1320 (1969).

[1.2] J. Weber, *Anisotropy and Polarization in the Gravitational-Radiation Experiments,* Phys. Rev. Lett. **25**, 180 (1970).

[1.3] J. Weber, *The Detection of Gravitational Waves,* Sci. Am. **224**, 22 (1971).

[1.4] J. Weber, *Computer Analyses of Gravitational Radiation Detector Coincidences,* Nature **240**, 28 (1972).

[1.5] A. Einstein, *Die Grundlagen der Allgemeinen Relativitätstheorie,* Annalen der Physik **49**, 769 (1916).

[1.6] C. Misner, K. S. Thorne, and J. A. Wheeler, *Gravitation,* W. H. Freeman, San Francisco (1973).

[1.7] B. F. Schutz, *Gravity from the Ground Up. An Introductory Guide to Gravity and General Relativity,* Cambridge University Press (2002).

[1.8] Most detectors provide their latest sensitivity curves on the web.
LIGO:
`http://www.ligo.caltech.edu/~lazz/distribution/LSC_Data/`
GEO600:
`http://www.geo600.uni-hannover.de/geocurves/`
VIRGO:
`http://wwwcascina.virgo.infn.it/DataAnalysis/`

[1.9] A. Vinante et al., *Present performance and future upgrades of the AURIGA capacitive readout,* Class. Quantum Grav. **23**, S103 (2006).

[1.10] P. Astone et al., *Status report on the EXPLORER and NAUTILUS detectors and the present science run,* Class. Quantum Grav. **23**, S57 (2006).

[1.11] O. D. Aguiar et al., *The Brazilian gravitational wave detector Mario Schenberg: status report,* Class. Quantum Grav. **23**, S239 (2006).

[1.12] A. de Waard et al., *Preparing for science run 1 of MiniGRAIL,* Class. Quantum Grav. **23**, S79 (2006).

[1.13] V. B. Braginsky, A. B. Manukin, E. I. Popov, and V. N. Rudenko, *Search for Gravitational Radiation of Extra-Terrestrial Origin,* JETP Lett. **16**, 108 (1972).

[1.14] J. L. Levine, and R. L. Garwin, *Absence of Gravity-Wave Signals in a Bar at 1695 Hz,* Phys. Rev. Lett. **31**, 173 (1973).

[1.15] J. A. Tyson, *Null Search for Bursts of Gravitational Radiation,* Phys. Rev. Lett. **31**, 326 (1973).

[1.16] D. Bramanti, K. Maischberger, and D. Parkinson, *Optimization and Data Analysis of the Frascati Gravitational-Wave Detector,* Lettere al Nuovo Cimento **7**, 665 (1973).

[1.17] R. W. P. Drever, J. Hough, R. Bland, and G. W. Lesnoff, *Search for Short Bursts of Gravitational Radiation,* Nature **246**, 340 (1973).

[1.18] M. E. Gerstenshtein and V. I. Pustovoit, *On the Detection of Low Frequency Gravitational Waves,* Soviet Physics-JETP **16**, 433 (1963) [Originally published in Russian 1962].

[1.19] H. Collins, *Gravity's shadow: the search for gravitational waves,* The University of Chicago Press, Chicago (2004).

[1.20] G. E. Moss, L. R. Miller, and R. L. Forward, *Photon-noise-limited laser tranducer for gravitational antenna,* Appl. Opt. **10**, 2495 (1971).

[1.21] R. L. Forward, *Wideband laser-interferometer graviational-radiation experiment,* Phys. Rev. D **17**, 379 (1978).

[1.22] R. Weiss, *Electromagnetically Coupled Broadband Gravitational Antenna,* RLE Quarterly Progress Report **105**, 54 (1972).

[1.23] G. Heinzel, K. A. Strain, J. Mizuno, K. D. Skeldon, B. Willke, W. Winkler, R. Schilling, A. Rüdiger, and K. Danzmann, *Experimental demonstration of a suspended dual recycling interferometer for gravitational wave detection,* Phys. Rev. Lett. **81**, 5493 (1998).

[1.24] A. Abramovici, W. E. Althouse, R. W. P. Drever, Y. Gürsel, S. Kawamura, F. J. Raab, D. Shoemaker. L. Sievers, R. E. Spero, K. S. Thorne, R. E. Vogt, R. Weiss, S. E. Whitcomb, and M. E. Zucker, *LIGO: The Laser Interferometer Gravitational-Wave Observatory,* Science **256**, 325 (1992).

[1.25] `http://www.lsc.org`

[1.26] `https://ligo.gravity.psu.edu/roster/`

[1.27] B. Caron et al. *The Virgo interferometer* Class. Quantum Grav. **14**, 1461 (1997).

[1.28] G. Leuchs, K. Maischberger, A. Rüdiger, R. Schilling, L. Schnupp, and W. Winkler, *Proposal for the Construction of a Large Laser Interferometer for the Measurement of Gravitational Waves,* MPQ-Report **131**, (1987).

[1.29] B. Willke et al., *The GEO 600 gravitational wave detector,* Class. Quantum Grav. **19**, 1377 (2002).

[1.30] S. Goßler, *The suspension systems of the interferometric gravitational-wave detector GEO600,* Ph.D. thesis, Universität Hannover (2004).

[1.31] H. Grote et al., *Dual recycling for GEO 600,* Class. Quantum Grav. **21**, S473 (2004).

[1.32] K. Kawabe et al., *Status of TAMA project,* Class. Quantum Grav. **14**, 1477 (1997).

[1.33] F. Acernese et al., *The Virgo status,* Class. Quantum Grav. **23**, S635 (2006).

[1.34] `http://www.ligo.caltech.edu/advLIGO/`

[1.35] M. Punturo, *Virgo: Plans for the Next Future,* Gravitational Wave Advanced Detector Workshop, Elba (2006), slides available at
`http://www.ligo.caltech.edu/docs/G/G060332-00/`

[1.36] B. Willke et al., *The GEO-HF project,* Class. Quantum Grav. **23**, S207 (2006).

[1.37] D. Blair, *Proposal to Extend Current AIGO High Optical Power Research Facility to a 5km Advanced Interferometer,* Gravitational Wave Advanced Detector Workshop, Elba (2006), slides available at
`http://www.ligo.caltech.edu/docs/G/G060284-00.ppt`

[1.38] K. Kuroda et al., *The status of LCGT,* Class. Quantum Grav. **23**, S215 (2006).

[1.39] K. S. Thorne, *Karl Schwarzschild Lecture: Gravitational Radiation - A New Window Onto the Universe,* in Rev. Mod. Astr. **10**, ed. R. E. Schielicke, Astronomische Gesellschaft (1997).

[1.40] G. Heinzel, C. Braxmaier, K. Danzmann, P. Gath, J. Hough, O. Jennrich, U. Johann, A. Rüdiger, M. Sallusti, and H. Schulte, *LISA interferometry: recent developments,* Class. Quantum Grav. **23**, S119 (2006).

[1.41] R. W. P. Drever, *Concepts for Extending the Ultimate Sensitivity of Interferometric Gravitational Wave Detectors Using Non-Transmissive Optics with Diffractive or Holographic Coupling,* in Proceedings of the Seventh Marcel Grossman Meeting on General Relativity, M. Keiser and R. T. Jantzen (eds.), World Scientific, Singapore (1995).

[1.42] K.-X. Sun and R. L. Byer, *All-reflective Michelson, Sagnac, and Fabry-Perot interferometers based on grating beam splitters,* Opt. Lett. **23**, 567 (1997).

[1.43] P. Beyersdorf, *personal communication.*

[1.44] S. Wise, G. Mueller, D. Reitze, D. B. Tanner, and B. F. Whiting, *Linewidth-broadened Fabry - Perot cavities within future gravitational wave detectors,* Class. Quantum Grav. **21**, S1031 (2004).

[1.45] Y. Chen, *Treatment of Grating Pairs Using Plane-Wave Approximation,* LSC Meeting, Livingston, LA (2004), slides available at
`http://www.ligo.caltech.edu/docs/G/G040194-00/`

[1.46] S. Wise, V. Quetschke, A. J. Deshpande, G. Mueller, D. H. Reitze, D. B. Tanner, B. F. Whiting, Y. Chen, A. Tünnermann, E. Kley, and T. Clausnitzer *Phase Effects in the Diffraction of Light: Beyond the Grating Equation,* Phys. Rev. Lett. **95**, 013901 (2005).

[1.47] G. R. Harrison, *The production of diffraction gratings I. Development of the ruling art,* J. Opt. Soc. Am. **39**, 413 (1949).

[1.48] A. Labeyrie and J. Flamand, *Spectrographic performance of holographically made diffraction gratings,* Opt. Comm. **1**, 5 (1969).

[1.49] J. A. Britten et al, *Advanced dielectric grating technology for high-energy petawatt lasers,* Quantum Electronics and Laser Science Conference **3**, 2035 (2005).

[1.50] E.-B. Kley, L.-C. Wittig, A. Tünnermann, *Microstructure technology for optical component fabrication,* in Microoptics. From technology to applications, ed. J. Jahns, Springer, New York (2004).

[1.51] D. Herriott, H. Kogelnik, and R. Kompfner, *Off-axis paths in spherical mirror interferometers,* Appl. Opt. **3**, 523 (1964).

[1.52] B. J. Meers, *Recycling in laser-interferometric gravitational-wave detectors,* Phys. Rev. D **38**, 2317 (1988).

[1.53] J. Mizuno, K. A. Strain, P. G. Nelson, J. M. Chen, R. Schilling, A. Rüdiger, W. Winkler, and K. Danzmann, *Resonant sideband extraction: a new configuration for interferometric gravitational wave detectors,* Phys. Lett. A **175**, 273 (1993).

[1.54] Y. Chen, *Sagnac interferometer as a speed-metertype, Quantum-Nondemolition gravitational-wave detector,* Phys. Rev. D **67**, 122004 (2003).

[1.55] V. B. Braginsky, F.A. Khalili, *Gravitational wave antenna with QND speed meter,* Phys. Lett. A **147**, 251 (1990).

[1.56] C. M. Caves, *Quantum-mechanical noise in an interferometer,* Phys. Rev. D **23**, 1693 (1981).

[1.57] H. Vahlbruch, S. Chelkowski, B. Hage, A. Franzen, K. Danzmann, R. Schnabel, *Coherent Control of Vacuum Squeezing in the Gravitational-Wave Detection Band,* Phys. Rev. Lett. **97**, 011101 (2006).

[1.58] S. A. Furman and A. V. Tikhonravov, *Basics of optics of multilayer systems,* Gif-sur-Yvette: Ed. Frontires (1992).

[1.59] E. D'Ambrosio, *Nonspherical mirrors to reduce thermoelastic noise in advanced gravitational wave interferometers,* Phys. Rev. D **67**, 102002 (2003).

[1.60] `http://www.ligo.caltech.edu/~gari/index.htm`

[1.61] S. Hild, H. Lück, W. Winkler, K. A. Strain, H. Grote, J. R. Smith, M. Malec, M. Hewitson, B. Willke, J. Hough, K. Danzmann, *Measurement of a low-absorption sample of OH-reduced fused silica,* Appl. Opt. **45**, 7269 (2006).

[1.62] The VIRGO Collaboration et al., *The VIRGO large mirrors: a challenge for low loss coatings,* Class. Quantum Grav. **21**, S935 (2004).

[1.63] P. Hello, J. Y. Vinet, *Analytical models of transient thermoelelastic deformations of mirrors heated by high power cw laser beams,* J. Phys. **51**, 2243 (1990).

[1.64] W. Winkler, K. Danzmann, A. Rüdiger, R. Schilling, *Heating by optical absorption and the performance of interferomtric gravitational-wave detectors*, Phys. Rev. A **44**, 7022 (1991).

[1.65] K. A. Strain, K. Danzmann, J. Mizuno, P. G. Nelson, A. Rüdiger, R. Schilling, W. Winkler, *Thermal lensing in recycling interferometric gravitational wave detectors,* Phys. Lett. A **194**, 124 (1994).

[1.66] R. C. Lawrence, *Active Wavefront Correction in Laser Interferometric Gravitational Wave Detectors,* Ph.D. thesis, Massachusetts Institute of Technology (2003).

[1.67] D. Shoemaker, *Ground-based interferometric gravitational-wave detectors in the LISA epoch,* Class. Quantum Grav. **20**, S11 (2003).

[1.68] S. A. Hughes and K. S. Thorne, *Seismic gravity-gradient noise in interferometric gravitational-wave detectors,* Phys. Rev. D **58**, 122002 (1998).

[1.69] Y. Levin, *Internal thermal noise in the LIGO test masses: A direct approach,* Phys. Rev. D **57**, 659 (1998).

[1.70] V. B. Braginsky, M. L. Goredetsky, and S. P. Vyatchanin, *Thermodynamical fluctuations and photo-thermal shot noise in gravitational wave antennae,* Phys. Lett. A **264**, 1 (1999).

[1.71] Y. T Liu, K. S. Thorne, *Thermoelastic noise and homogeneous thermal noise in finite size gravitational wave test masses,* Phys. Rev. D **62**, 122002 (2000).

[1.72] G. M. Harry et al., *Thermal noise from optical coatings in gravitational wave detectors,* Appl. Opt. **45**, 1569 (2006).

[1.73] S. Miyoki et al., *The CLIO project,* Class. Quantum Grav. **23**, S231 (2006).

[1.74] T. Uchiyama et al., *Mechanical quality factor of a cryogenic sapphire test mass for gravitational wave detectors,* Phys. Lett. A **261**, 5 (1999).

[1.75] S. Rowan R. L. Byer, M. M. Fejer, R. Route G. Cagnoli, D. R. M. Crooks, J. Hough, P. Sneddon, and W. Winkler, *Test mass materials for a new generation of gravitational wave detectors,* Proc. SPIE **4856**, 292 (2003).

[1.76] P. Beyersdorf, *The polarization Sagnac interferometer for gravitational wave detection,* Ph.D. thesis, Stanford University (2001).

[1.77] O. Burmeister, *Fabry-Perot Resonatoren mit diffraktiven Einkopplern,* Diplomarbeit, Universität Hannover (2005).

[1.78] E. G. Loewen and E. Popov, *Diffraction gratings and applications,* Marcel Dekker, New York (1997).

[1.79] The authors of [1.42] reference an earlier proposal [1.80], whose existence could unfortunately not be confirmed by the author of this thesis.

[1.80] R. L. Byer, in Gravitational Astronomy: Instrument Design and Astrophysical Prospects, D. E. McClelland and H.-A. Bachor (eds.), World Scientific, Singapore, (1990).

[1.81] The demonstration of a ring resonator concept based on a low diffraction grating is briefly mentioned in [1.76], but no thorough investigation of its properties was performed [1.43].

[1.82] S. Fahr, *Gitter für die interferometrische Gravitationswellendetektion,* Diplomarbeit, Universität Jena (2006).

[1.83] D. Friedrich, *Michelson Interferometer mit diffraktivem Strahlteiler,* Diplomarbeit, Universität Hannover (2006).

[1.84] D. Rosenblatt, A. Sharon, and A. A. Friesem *Resonant Grating Waveguide Structures,* IEEE J. Quantum Electron. **33**, 2038 (1997).

[1.85] E. Popov and Bozhan Bozhkov, *Corrugated waveguides as resonance optical filters - advantages and limitations,* J. Opt. Soc. Am. A **18**, 1758 (2001).

Chapter 2

Optical characterization of ultrahigh diffraction efficiency gratings

We report on the optical characterization of an ultrahigh diffraction efficiency grating in a first-order Littrow configuration. The apparatus used was an optical cavity built from the grating under investigation and an additional high reflection mirror. Measurement of the cavity finesse provided precise information about the grating's diffraction efficiency and its optical loss. We measured a finesse of 1580 from which we deduced a diffraction efficiency of $(99.635 \pm 0.016)\,\%$ and an overall optical loss due to scattering and absorption of just $0.185\,\%$. Such high quality gratings, including the tool used for their characterization, might apply for future gravitational wave detectors. For example the demonstrated cavity itself presents an all-reflective, low-loss Fabry-Perot resonator that might replace conventional arm cavities in advanced high power Michelson interferometers.

Originally published as A. Bunkowski et al., Appl. Opt. **45**, 5795 (2006).

2.1 Introduction

High-quality optics are key devices in laser interferometric precision measurements. Especially for high-power laser applications with nested cavities, such as in gravitational wave detectors [2.1], mirrors with high reflectivity and low overall optical loss are essential. Mirrors with a power reflectance greater than 99.9998 % for a given laser wavelength have been reported [2.2]. The overall optical loss consisting of stray light from the surface, transmission, and absorption in the coating was as low as 1.6 ppm [2.2].

Gratings are traditionally used in applications in which one wants to spatially resolve different optical wavelengths, e.g., in spectrographs or pulse compressors-stretchers for short-pulse laser systems. In these applications, high diffraction efficiency over a range of optical wavelengths is desired. Dielectric reflection gratings with diffraction efficiencies of 96 %, 97 %, and 99 % have been reported [2.3–2.5]. However, the measurement techniques used in those applications allowed for only a rough estimation of the diffraction efficiency, and no error bars for the values were given. Diffraction gratings may also be used in advanced high-power laser interferometers [2.6, 2.7], where they allow for the all-reflective realization of beam splitters and cavity couplers, and therefore may help to reduce thermal effects in the substrate, such as thermal lensing [2.8] and thermorefractive noise [2.9]. In interferometric applications, monochromatic laser light is used, and the wavelength dispersive property of the gratings is not essential. The point of interest lies in the number and the properties of the reflective diffraction ports and their couplings that determine the interference between input beams. Two different all-reflective resonator concepts have been demonstrated to date. High-efficiency gratings in first-order Littrow configuration form cavity couplers with two ports analogous to partially transmitting mirrors [2.7]. Low-efficiency gratings in second-order Littrow configuration can be used as low-loss couplers with three ports [2.10]. Analogous to conventional mirrors, however, optical loss in terms of scattering or absorption has to be minimized in order to gain maximum laser power buildup and measurement sensitivity. The question therefore arises as to whether high-efficiency gratings with highly corrugated surfaces will ever be able to fulfill the strict low scattering loss requirements.

In this paper we report on the optical characterization of a high-efficiency grating in view of applications in interferometry. The grating was used in a first-order Littrow configuration to couple laser light into a Fabry-Perot cavity with a measured finesse of 1580 ± 60. This experiment allowed for the accurate measurement of both the grating's loss and the diffraction efficiency. The latter one was determined to be $(99.635 \pm 0.016)\,\%$. To our knowledge this is the highest and most accurately determined value reported in the literature.

The grating device was designed for a laser wavelength of 1064 nm and a Littrow angle of approximately 30°. The grating structure had rectangular grooves with a period of 1060 nm. For fabrication we used electron-beam direct writing (electron-beam writer LION LV1, Leica Microsystems GmbH) and reactive ion beam etching into the top layer of a highly reflective dielectric multilayer stack. The stack consisted of 36 alternating layers of 195 nm SiO_2 and 136 nm Ta_2O_5 placed on a fused-silica substrate with a surface flatness of $\lambda/10$. For the theoretical optimization of the grating we used the rigorous coupled-wave analysis [2.11]. To ensure good reproducibility and homogeneity over the whole grating area, an important concern of the design was a large groove parameter tolerance of diffraction efficiency. By using SiO_2 with a thickness of 1.12 μm as the top layer of the dielectric stack the theoretical design exhibited a diffraction efficiency of more than 99 % for groove depths between 700 nm and 850 nm and groove widths between 530 nm and 760 nm.

2.2 Experimental Procedure

A schematic of our experiment is seen in Fig. 2.1. The light source used was a 1.2 W diode-pumped Nd:YAG laser at 1064 nm (Model Mephisto, Innolight GmbH). Before the s-polarized laser beam was sent into the grating cavity it was spatially filtered with a triangular ring cavity (mode cleaner) [2.12]. The highly reflective end mirror of the grating cavity was mounted on a piezoelectric transducer (PZT) which was used either to scan or to actively control the cavity length. The error signal for the electronic servo loop was obtained from the cavity transmission demodulated at the phase modulation frequency introduced by the electro-optical modulator (EOM).

In a first-order Littrow configuration, only two diffraction orders exist, and the

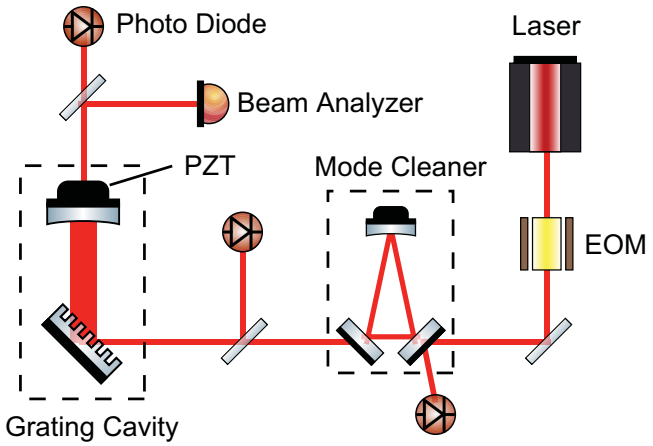

Figure 2.1: (Experimental setup; EOM, electro optical modulator; PZT, cavity mirror with piezoelectric transducer for length control.

grating (subscript 1) is characterized by the zeroth and first-order amplitude diffraction efficiencies r_1 and η_1, respectively, as well as the loss amplitude l_1. Similarly, the cavity end mirror (subscript 2) is described by r_2, t_2 and l_2. Energy conservation implies

$$r_1^2 + \eta_1^2 + l_1^2 = 1, \tag{2.1}$$

$$r_2^2 + t_2^2 + l_2^2 = 1\,. \tag{2.2}$$

Figure 2.2 shows the transmission spectrum of the cavity as the PZT is linearly scanned over one free spectral range of the cavity. In addition to the peaks of the fundamental mode of the cavity there are only two smaller peaks from higher-order modes visible, indicating a good matching of laser beam and cavity mode.

A method to obtain a precise value for a mirror reflectance close to unity is a measurement of the finesse F of a cavity consisting of a mirror with a known reflectance and the one in question. For the first time, to the best of our knowledge, this method is applied to characterize a high-efficiency grating. If losses due to absorption in the space between the mirrors (which would appear additionally to l_1 and l_2) are neglected, the finesse F of a two mirror Fabry-Perot resonator depends on the reflectance of the two end mirrors only. In our case one of the end mirrors is a grating and the finesse can be approximated by

$$F = \pi(\eta_1 r_2)^{1/2}/(1 - \eta_1 r_2). \tag{2.3}$$

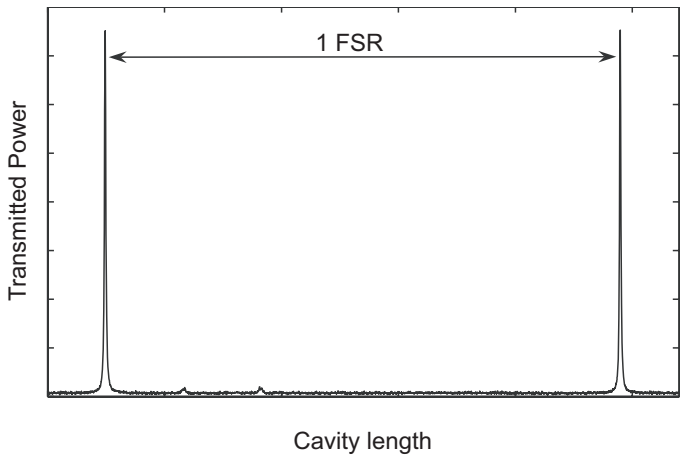

Figure 2.2: Transmitted power of the cavity. Photodiode signal behind the grating cavity as the cavity is linearly scanned over one free spectral range (FSR).

For a cavity of length L its free spectral range is given by $f_{\mathrm{FSR}} = c/2L$ where c is the speed of light. The ratio of f_{FSR} to the FWHM f_{FWHM} of the Airy transmission spectrum peaks determines the finesse

$$F = f_{\mathrm{FSR}}/f_{\mathrm{FWHM}}. \tag{2.4}$$

The length of the cavity was measured to $L = (94 \pm 1)\,\mathrm{mm}$, resulting in $f_{\mathrm{FSR}} \approx 1.6\,\mathrm{GHz}$. The cavity linewidth was measured by utilizing frequency marker signals. The laser light was phase modulated at $f_{\mathrm{mod}} = 4\,\mathrm{MHz}$ by using an EOM. The ac output of the photodiode in front of the grating cavity was then demodulated at f_{mod}. For the correct demodulation phase this signal shows a minimum and a maximum at exactly $\pm f_{\mathrm{mod}}$ and can be used to calibrate the x axis in Fig. 2.3. The figure shows a typical measured dc signal for the photodiode behind the cavity as well as the marker signals at $f_{\mathrm{marker}} = \pm(4 \pm 0.04)\,\mathrm{MHz}$ while the cavity was linearly scanned with 1 kHz repetition rate. The uncertainty in the position of the marker signal is due to an error in the demodulation phase. A fit of the transmission signal to the well-known Airy function of cavities permitted the calculation of the width of the transmission peak. Due to nonlinearities in the PZT and acoustic vibrations, there is a statistical variation of the linewidth of the peak. We averaged over 75 measurements by using different operating points of the PZT and we could reduce the statistical error in the peak width

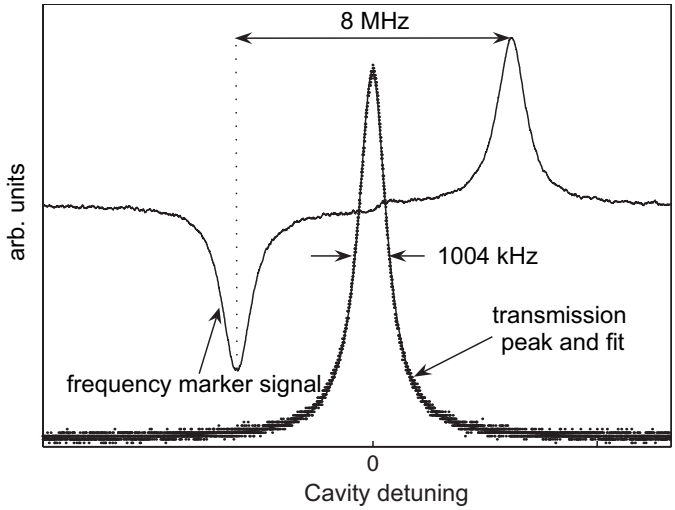

Figure 2.3: Scan over one cavity transmission peak. The x axis was calibrated with $\pm\,4\,\mathrm{MHz}$ marker signals.

to $\pm\,3.5\,\%$.

With Eq. (2.4) we could calculate the finesse of the cavity $F = 1580 \pm 60$. The cavity end mirror was superpolished and coated by Research Electro-Optics, Inc., and specified to have values of $t_2^2 = 300 \pm 30$ ppm and $l_2^2 < 30\,\mathrm{ppm}$. From these specifications we estimated the mirror's reflectivity to $r_2^2 = (99.9685 \pm 0.0034)\,\%$. With Eqs. (2.2) and (2.3) we obtained $\eta_1^2 = (99.635 \pm 0.016)\,\%$ for the grating's first-order diffraction efficiency. The error in η_1^2 results from an error propagation of each known uncertainty of the quantities L, f_{marker}, fitted peak width, and r_2^2 as shown in Table 1. The specular reflection of the grating was measured independently with a calibrated power meter to be $r_1^2 = (0.18 \pm 0.009)\,\%$. Hence we calculated the overall loss of the grating according to Eq. (2.1) to be $l_1^2 = (0.185 \pm 0.025)\,\%$. We emphasize that this loss contained all contributions from scattering, absorption, transmission, and higher diffraction orders. To the best of our knowledge, this result presents the lowest and most accurately determined grating loss reported in the literature. The previous results were those by Perry *et al.* [2.3] and Hehl *et al.* [2.4], who reported a 1.5 % and a 1 - 2 % loss, respectively. Destouches *et. al.* [2.5] did not comment on the loss.

In addition to the grating's loss we also investigated its influence on the laser

Table 2.1: Error propagation

Quantity	error	proj. error for η_1^2 [ppm]
L	± 1 mm	± 48
f_{marker}	± 40 kHz	± 43
peak width	± 3.5 %	± 143
r_2^2	± 34 ppm	± 34
Total RMS error expected		± 160

beam's spatial profile. Again a cavity in first-order Littrow configuration was set up with a cavity mode waist on the grating's surface now using an end mirror with power reflectivity $r_2^2 = 99\,\%$ to reduce the finesse value and to increase transmission. The cavity length was controlled by use of a Pound-Drever-Hall locking scheme with a phase modulation sideband frequency of 4 MHz. The beam profile for the horizontal and vertical directions was measured after the cavity by using a seven-blade tomographic profiler (SuperBeamAlyzer, Melles Griot) fitted with a Gaussian model, as shown in Fig. 2.4. The sum of the absolute differences between the value of every measured point and the fitted function divided by the sum of the values of all fitted points is a measure of how much beam power can be represented by a Gaussian function. For both directions we obtained values of greater than 99%. For this experiment, the mode cleaner had been taken out, which allowed us to observe a mode-cleaning effect from the grating cavity. We characterized the laser beam behind the EOM by using the same apparatus and got spatial profiles that were described by a Gaussian function by only 98 %.

2.3 Conclusion

We presented a detailed characterization of diffraction efficiency and overall loss of a grating in a first-order Littrow mount. The grating's diffraction efficiency showed an outstanding high value that permitted the construction of a high-finesse cavity as a characterizing tool. The value of the finesse was limited by the first-order diffraction

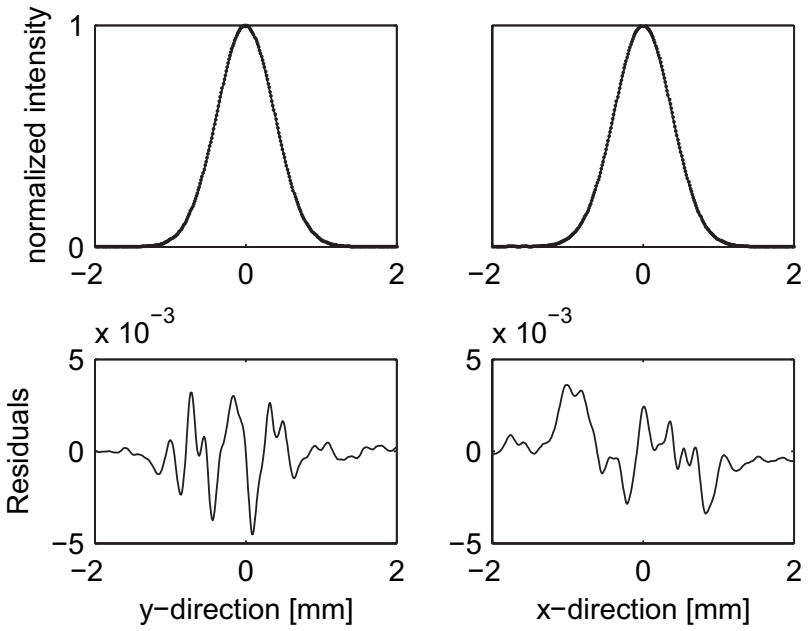

Figure 2.4: Spatial beam profile of the laser beam after the cavity for horizontal (perpendicular to the grating lines) and vertical (parallel to the grating lines) direction. Top, measured points (dots) and best gaussian fit (solid curve); bottom, Residuals between measurement and fit.

efficiency. This is in contrast to Ref. [2.10] in which a low diffraction efficiency grating was characterized with a high-finesse cavity and the limit for the finesse was given by the specular reflectivity of the grating. Our approach is a valuable diagnostic tool to improve future techniques of grating fabrication since all types of loss are simultaneously detected. We expect that with improved technology high grating efficiencies with simultaneously low loss are possible and that they will even fulfill the strict requirements of future interferometers, such as those for gravitational wave detection.

This work was supported by the Deutsche Forschungsgemeinschaft within the Sonderforschungsbereich TR7.

References

[2.1] B. Abbott et al., *Detector description and performance for the first coincidence observations between LIGO and GEO,* Nuclear Instruments and Methods in Physics Research A **517**, 154 (2004).

[2.2] G. Rempe, R. J. Thompson, H. J. Kimble, and R. Lalezari, *Measurement of ultralow losses in an optical interferometer,* Opt. Lett. **17**, 363 (1992).

[2.3] M. D. Perry, R. D. Boyd, J. A. Britten, D. Decker, B. W. Shore, C. Shannon, and E. Shults, *High-efficiency multilayer dielectric diffraction gratings,* Opt. Lett. **20**, 940 (1995).

[2.4] K. Hehl, J. Bischoff, U. Mohaupt, M. Palme, and B. Schnabel, *High-efficiency dielectric reflection gratings: design, fabrication, and analysis,* Appl. Opt. **38**, 6257 (1999).

[2.5] N. Destouches, A. V. Tishchenko, J. C. Pommier, S. Reynaud, O. Parriaux, S. Tonchev, and M. Abdou Ahmed, *99% efficiency measured in the -1st order of a resonant grating,* Opt. Expr. **13**, 3230 (2005).

[2.6] R. W. P. Drever, *Concepts for Extending the Ultimate Sensitivity of Interferometric Gravitational Wave Detectors Using Non-Transmissive Optics with Diffractive or Holographic Coupling,* in Proceedings of the Seventh Marcel Grossman Meeting on General Relativity, M. Keiser and R. T. Jantzen (eds.), World Scientific, Singapore (1995).

[2.7] K.-X. Sun and R. L. Byer, *All-reflective Michelson, Sagnac, and Fabry-Perot interferometers based on grating beam splitters,* Opt. Lett. **23**, 567 (1997).

[2.8] W. Winkler, K. Danzmann, A. Rüdiger, and R. Schilling, *Heating by optical absorption and the performance of interferometric gravitational-wave detectors,* Phys. Rev. A **44**, 7022 (1991).

[2.9] V. B. Braginsky, M. L. Gorodetsky, and S. P. Vyatchanin, *Thermo-refractive noise in gravitational wave antennae,* Phys. Lett. A **271**, 303 (2000).

[2.10] A. Bunkowksi, O. Burmeister, P. Beyersdorf, K. Danzmann, R. Schnabel, T. Clausnitzer, E.-B. Kley, and A. Tünnermann, *Low-loss grating for coupling to a high-finesse cavity,* Opt. Lett. **29**, 2342 (2004).

[2.11] M. G. Moharam, and T. K. Gaylord, *Diffraction analysis of dielectric surface-relief gratings,* J. Opt. Soc. Am. **72**, 1385 (1982).

[2.12] B. Willke, N. Uehara, E. K. Gustafson, R. L. Byer, P. J. King, S. U. Seel, and R. L. Savage, Jr., *Spatial and temporal filtering of a 10-W Nd:YAG laser with a Fabry Perot ring-cavity premode cleaner,* Opt. Lett. **23**, 1704 (1998).

Chapter 3

Low-loss grating for coupling to a high-finesse cavity

A concept for a low-loss all-reflective cavity coupler is experimentally demonstrated at a wavelength of 1064 nm. A 1450-nm period dielectric reflection grating with a diffraction efficiency of 0.58 % in the -1st order is used in 2nd-order Littrow configuration as a coupler to form a cavity with a finesse of 400. The application of such reflective low-loss cavity couplers in future generations of gravitational-wave detectors and implementation issues are discussed.

Originally published as A. Bunkowski et al., Opt. Lett. **29**, 2342 (2004).

An international network of first-generation, kilometer-scale, earthbound laser-interferometric gravitational-wave (GW) detectors, consisting of the Laser Interferometer Gravitational Wave Observatory (LIGO) [3.1, 3.2], GEO 600 [3.2], TAMA [3.3], and the VIRGO project [3.4], is currently moving from the commissioning phase to the long-term data-taking operational phase. These detectors are Michelson interferometers. Power recycling and arm cavities are two techniques being used to increase the laser power in the interferometer and hence the detector sensitivity. Both techniques utilize cavities to which laser light is coupled via a partially transmitting mirror. For first-generation detectors the light power inside the interferometer will be in the order of 10 kW at a wavelength of 1064 nm. To increase the detection sensitivity even

further, future GW interferometers will use light power of the order of megawatts for which heating effects in the transmissive elements become an issue. Power absorption in the substrates leads to thermal lensing and also to deformation of the optical surface. These distortions will limit the circulating power below the level that is necessary to optimize quantum noise. To reduce thermal noise, cryogenic techniques for the main optics are likely to be used in third-generation GW detectors. Absorbed heat in the substrates will worsen the cooling efforts of the optical elements. To avoid heating in the substrate, reflective-grating beam splitters can be used instead of partially transmissive mirrors and beam splitters [3.5]. An additional advantage of all-reflective optics within GW detectors is the elimination of the constraint that the substrate materials be optically transparent. Considering opaque substrate materials with superior mechanical properties allows one to lower the thermal noise in the detector.

In proof-of-principle experiments Sun and Byer [3.6] demonstrated Michelson and Sagnac interferometers based on all-reflective elements. They also demonstrated a Fabry-Perot coupler concept that is based on high-diffraction-efficiency gratings in the 1st-order Littrow configuration. Drever pointed out that low-diffraction-efficiency gratings could also be used as cavity couplers and argued that the overall losses should be lower than in high-diffraction efficiency elements. An all-reflective interferometer configuration that avoids the use of a 50/50 beam splitter and uses low diffraction-efficiency gratings and mirrors as the only major optical elements, as depicted schematically in Fig 3.1, was proposed [3.5]. But to our knowledge no experimental realization of interferometers utilizing low-diffraction gratings has been reported so far. In this Letter we report on the design of a low-loss diffraction grating with a diffraction efficiency of less than 1 % and on the experimental realization of a high-finesse linear cavity that uses the grating as a coupler.

For a laser beam of wavelength λ that is incident on a reflection grating the output angle Θ_m of the mth diffracted order is given by the well known grating equation

$$d(\sin\Theta_m - \sin\Theta_{\mathrm{in}}) = m\lambda, \tag{3.1}$$

where Θ_{in} is the incidence angle and d is the grating period. If it is used in the 1st-order Littrow configuration ($\sin\Theta_{\mathrm{in}} = \lambda/2d$), a reflection grating can be used as a cavity coupler [3.6]; the reflected (0th order) beam is used to couple light into the resonator.

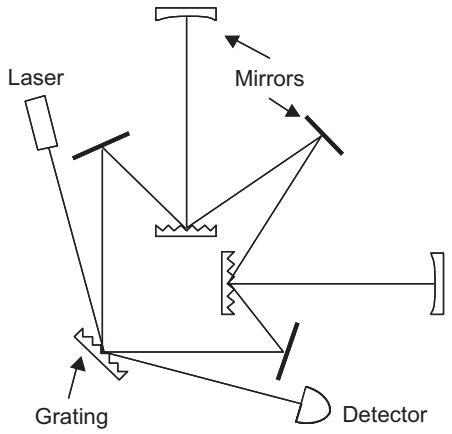

Figure 3.1: Interferometer setup proposed by Drever [3.5].

The finesse of such a resonator is limited by the maximum diffraction efficiency of the 1st order of the grating. However, if it is used in the 2nd-order Littrow configuration, as shown in Fig 3.2, the diffracted (-1st) order is used to couple the cavity. Then, the

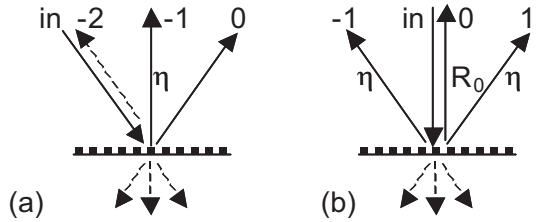

Figure 3.2: Reflected and transmitted orders from a reflection grating in the 2nd-order Littrow configuration: (a) Incident beam at the Littrow angle, (b) normal incidence.

maximum reflectivity R_0 of the grating under normal incidence is the limiting factor for the finesse of the cavity.

Standard coating techniques can routinely produce multilayers with a reflectivity greater than 99.98 %. This value is to be compared with routinely produced maximum diffraction efficiencies of about $\sim 95\,\%$ [3.7]. To our knowledge the highest value ever reported so far is also not greater than 99 % [3.8]. Therefore the 2nd-order Littrow configuration is the appropriate choice for efficient low-loss coupling to a linear resonator.

Every diffraction order that is allowed by the grating equation will contain some light power. To reduce overall losses in the device one should choose the grating period d so that only the diffraction orders that are going to be used are allowed by the grating equation. Only the ± 1 orders for normal incidence are needed in our case, which suggests that

$$\lambda < d < 2\lambda. \tag{3.2}$$

A common way of manufacturing high-efficiency dielectric reflection gratings is to etch a periodic structure into the top layer of a dielectric multilayer stack as it is done for the gratings used in high-power chirped-pulse amplification [3.9]. For the low diffraction efficiency grating needed for our application we used a different approach. We first etched the grating into a substrate and then overcoated it so that the dielectric layers effectively formed a volume grating, as can be seen from Fig 3.3. A shallow

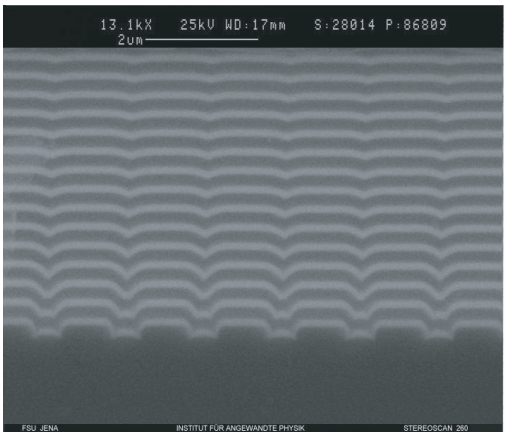

Figure 3.3: Cross section of an overcoated binary grating (SEM-image).

binary structure with a depth of 40–50 nm, a ridge width of 840 nm, and a period of $d = 1450$ nm was generated by electron-beam lithography and reactive ion-beam etching on top of a fused-silica substrate. The applied multilayer stack was composed of 32 alternating layers of silica (SiO_2) and tantalum pentoxide (Ta_2O_5). The diffraction efficiency of 1064-nm light with a polarization plane parallel to the grating grooves and perpendicular to the plane of incidence (s polarization) was measured to be $\eta = (0.58 \pm 0.04)\,\%$.

Figure 3.4 shows the experimental setup of the all-reflective Fabry-Perot cavity. A

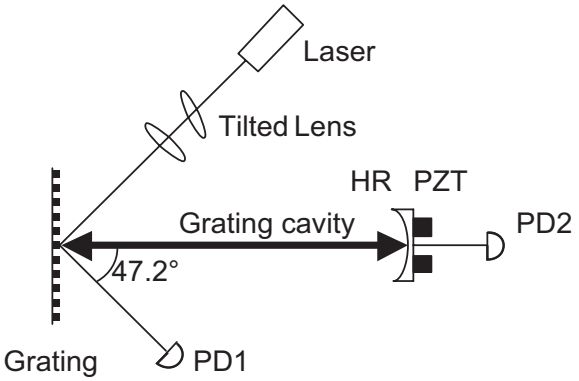

Figure 3.4: Experimental setup of the demonstrated grating Fabry-Perot cavity: HR, high reflector; PZT, piezoelectric transducer; PD1, PD2 photodiodes.

highly reflective mirror with a radius of curvature of 1.5 m mounted on a piezoelectric transducer to allow for cavity-length control was placed parallel to the grating surface at a distance of 43 cm. An s-polarized beam of 50 mW from a 1.2 W, 1064-nm diode-pumped Nd:YAG laser was used. The angle of incidence corresponded to 2nd-order Littrow configuration $\Theta_{in} = \arcsin(\lambda/d) \approx 47.2\,^{\circ}$. The circulating and reflected power from the cavity were observed by monitoring the leakage from the high reflector and from the 0th-order of the grating, respectively.

High circulating powers inside the cavity also demands good mode matching of input beam and cavity mode. Note that our grating couples modes at different angles of incident which changes the ratio of horizontal a vertical mode widths. The following relation holds for the horizontal width w_h of the beam

$$w_{\mathrm{in},h}/w_{m,h} = \cos\Theta_{\mathrm{in}}/\cos\Theta_m, \tag{3.3}$$

where in and m refer to the incoming and the diffracted beam, respectively. For our setup an input beam with an elliptical profile having a horizontal width of 1.47 times ($w_h/w_v = \cos\Theta_m/\cos\Theta_{\mathrm{in}} \approx 1.47$) the vertical width produced the desired round beam profile in the diffracted beam. The profile was generated by a pair of lenses from which one lens was tilted horizontally to have different focal lengths for the v and h directions.

Figure 3.5 shows the transmission and reflection interference fringes for the cavity

with a measured cavity finesse of 400 ± 20. More than 99 % of the power was measured

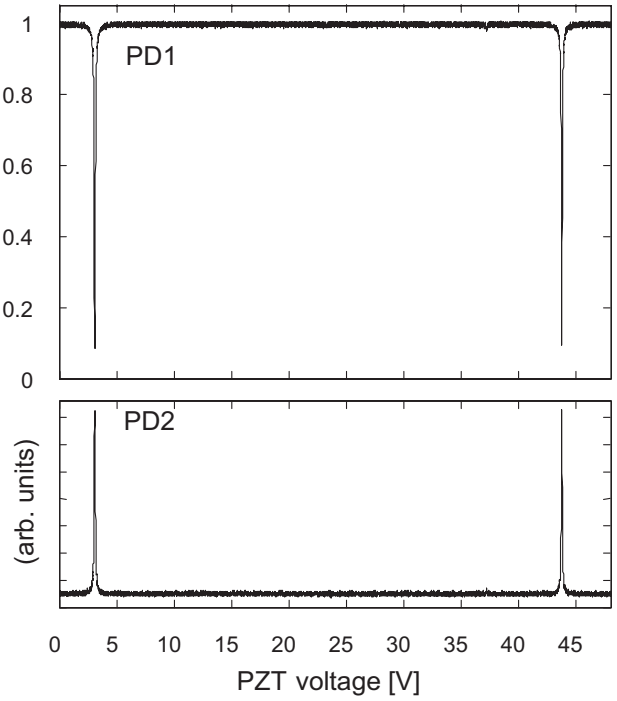

Figure 3.5: Measured signals of the two photodiodes according to Fig. 3.4 versus the piezoelectric transducer ramp voltage over one free spectral range. PD1, reflected power normalized to the power of the incident beam; PD2, circulating power in the cavity.

to be in the TEM_{00} mode, indicating excellent mode matching. With the measured value of the finesse and the known reflectance of the HR-mirror one can calculate the overall losses A which are defined by $A = 1 - R_0 - 2\eta$, where R_0 is the the reflectance for normal incidence. We find that $A = (0.38 \pm 0.2)\,\%$. Losses are due to transmitted orders and scattered light.

The partially transmissive mirrors conventionally used for coupling to a linear Fabry-Perot cavity can be considered two-port devices with simple phase relations between the two ports. The input coupler introduced here, however, is a three-port device. Light entering one port will always couple to all three ports. The phase relations of the light in the three different ports are more complex than in a two-port device. They depend on the diffraction efficiencies of the different orders and can be

calculated with a scattering matrix formalism [3.10]. Because of the additional port, new GW detector topologies can be obtained. The scheme shown in Fig. 3.1 for example, uses two linear grating cavities in the arms. On resonance these cavities will retroreflect most of the power incident on the grating, while the signal sidebands generated in the arms will be split equally between the two output ports of the cavity. Therefore the power and the signal are taking different paths in the interferometer. A detailed analysis of the phases of the three ports of the coupler as well as their effects on the properties of the proposed interferometer is in preparation and will be presented in the future.

In conclusion, we have experimentally demonstrated that a low-efficiency grating can be used as a cavity input coupler with low loss. A cavity with a finesse of 400 was constructed that far exceeded the best finesse values for an all-reflective cavity that had been previously reported [3.6]. We plan to optimize the design and manufacturing process of the gratings to produce gratings with even lower diffraction efficiency and overall losses. These gratings will have high potential to be implemented in future GW detector configurations.

This research was supported by the Deutsche Forschungsgemeinschaft within the Sonderforschungsbereich TR7.

References

[3.1] A. Abramovici, W. E. Althouse, R. W. P. Drever, Y. Gürsel, S. Kawamura, F. J. Raab, D. Shoemaker. L. Sievers, R. E. Spero, K. S. Thorne, R. E. Vogt, R. Weiss, S. E. Whitcomb, and M. E. Zucker, *LIGO: The Laser Interferometer Gravitational-Wave Observatory,* Science **256**, 325 (1992).

[3.2] B. Abbott et al., *Detector description and performance for the first coincidence observations between LIGO and GEO,* Nuclear Instruments and Methods in Physics Research A **517**, 154 (2004).

[3.3] M. Ando et al., *Stable Operation of a 300-m Laser Interferometer with Sufficient Sensitivity to Detect Gravitational-Wave Events within Our Galaxy,* Phys. Rev. Lett. **86**, 3950 (2001).

[3.4] F. Acernese et al., *Status of VIRGO,* Class. Quantum Grav. **21**, S385 (2004).

[3.5] R. W. P. Drever, *Concepts for Extending the Ultimate Sensitivity of Interferometric Gravitational Wave Detectors Using Non-Transmissive Optics with Diffractive or Holographic Coupling,* in Proceedings of the Seventh Marcel Grossman Meeting on General Relativity, M. Keiser and R. T. Jantzen (eds.), World Scientific, Singapore, (1995).

[3.6] K.-X. Sun and R. L. Byer, *All-reflective Michelson, Sagnac, and Fabry-Perot interferometers based on grating beam splitters,* Opt. Lett. **23**, 567 (1997).

[3.7] T. Clausnitzer, J. Limpert, K. Zöllner, H. Zellmer, H.-J. Fuchs, E.-B. Kley, A. Tünnermann, M. Jupé, and D. Ristau, *Highly efficient transmission gratings in fused silica for CPA systems,* Appl. Opt. **42**, 6934 (2003).

[3.8] J. A. Britten, S. J. Bryan, L. J. Summers, H. T. Nguyen, B. W. Shore, and O. Lyngnes, *Large Aperture, High-Efficiency Multilayer Dielectric Reflection Gratings*, in Proceedings of IEEE Conference on Lasers and Electro-Optics, CPDB7-1 Opt. Soc. America, Washington (2002).

[3.9] B. W. Shore, *Design of high-efficiency dielectric reflection gratings,* J. Opt. Soc. Am. A. **14**, 1124 (1997).

[3.10] A. Siegman, *Lasers* University Science Books, Sausalito (1986).

Chapter 4

Input-output relations for a three-port grating coupled Fabry-Perot cavity

We analyze an optical three-port reflection grating by means of a scattering matrix formalism. Amplitude and phase relations among the three ports, i.e., the three orders of diffraction, are derived. Such a grating can be used as an all-reflective, low-loss coupler to Fabry-Perot cavities. We derive the input-output relations of a three-port grating coupled cavity and find distinct properties that are not present in two-port coupled cavities. The cavity relations further reveal that the three-port coupler can be designed such that the additional cavity port interferes destructively. In this case the all-reflective, low-loss, single-end Fabry-Perot cavity becomes equivalent to a standard transmissive, two-port coupled cavity.

Originally published as A. Bunkowski et al., Opt. Lett. **30**, 1183 (2005).

In a recent experiment a three-port reflection grating coupled Fabry-Perot cavity with high Finesse was demonstrated [4.1]. The experiment was motivated by the idea that a three-port reflection grating should be able to provide two important features for advanced interferometry: low overall optical loss and no light transmission through optical substrates [4.2]. In advanced interferometers, such as in gravitational-wave

detectors, these couplers might be crucial for achieving the optimal combination of extremely high-power laser fields, materials with a high mechanical quality factor for suspended optics, and cryogenic temperatures to reduce optics and suspension thermal noise [4.3]. Previously, a different concept for all-reflective linear Fabry-Perot cavities based on a two-port reflection grating was experimentally demonstrated [4.4]. In this approach the reflection grating was used in a first-order Littrow mount where the input-output relations of the cavity are analogous to those of a conventional cavity with transmissive mirrors. The major disadvantage of this concept is, however, that it relies on high first-order diffraction efficiency requiring deep grating structures that are associated with high scattering losses. Contrary to this, the concept demonstrated in reference [4.1] used a second-order Littrow mount and relies on low first-order diffraction efficiency that can be achieved by very shallow grating structures with smaller scattering losses. The latter approach is therefore better suited for low-loss couplers to high-finesse cavities, a stringent requirement in high-power laser interferometry. A grating used in second-order Littrow mount, however, has three coupled ports in contrast with mirrors in which one input port is only coupled to two output ports. Knowledge of the phase relations of the three ports is essential for derivation of the input-output relations of the cavity.

In this letter we derive the amplitude and phase relations of an optical three-port device by means of the scattering matrix formalism. We restrict ourselves to a symmetric coupling between port 2 and the other two ports 1 and 3 described by η_1 (see Fig. 4.1). Generally, optical devices such as mirrors and beam splitters can be described by a complex-valued $n \times n$ scattering matrix $\mathbf{S}$ [4.5], where n input ports are represented by a vector $\mathbf{a}$ with the components a_i that are the complex amplitudes of the incoming waves at the ith port. The outgoing amplitudes b_i are represented by the vector $\mathbf{b}$. The coupling of input and output ports is given by

$$\mathbf{b} = \mathbf{S} \times \mathbf{a}\,. \tag{4.1}$$

For a lossless device $\mathbf{S}$ must be unitary. Reciprocity of the device demands $|S_{ij}| \equiv |S_{ji}|$, where S_{ij} denotes an element of the matrix $\mathbf{S}$. The magnitudes of the scattering coefficients are unique for a given device. The phase angles of the matrix elements, however, can be changed by choosing different reference planes in the various input and out-

put arms. One can therefore derive different scattering matrices for the same device. Nevertheless, certain phase relationships between the different coefficients must be maintained. Transmissive mirrors are commonly used to couple light into Fabry-Perot cavities. The input-output relations of such cavities are well understood. Essential for their derivation is the knowledge of the phase relations at the mirrors for the reflected and transmitted beams. A conventional two-coupled-port mirror with amplitude reflectance ρ and transmittance τ, for example, is generally described by

$$\mathbf{S_{2p}} = \begin{pmatrix} \rho & \tau \\ \tau & -\rho \end{pmatrix} \quad , \quad \mathbf{S_{2p}} = \begin{pmatrix} \rho & i\tau \\ i\tau & \rho \end{pmatrix}. \tag{4.2}$$

Using either one of these matrices, one can derive the amplitude reflectance r_{FP} and transmittance t_{FP} of a cavity consisting of two partially transmitting mirrors with reflectivities ρ_0, ρ_1. The length of the cavity is expressed by the tuning parameter $\phi = \omega L/c$, where ω is the angular frequency of the light and c the speed of light, thus one obtains

$$r_{\mathrm{FP}} = [\rho_0 - \rho_1 \exp(2i\phi)]d\,, \tag{4.3}$$

$$t_{\mathrm{FP}} = -\tau_0\tau_1 \exp(-i\phi)d\,, \tag{4.4}$$

where $\rho_{0,1}$ and $\tau_{0,1}$ denote the reflectance and transmittance of the two cavity mirrors, respectively, and we introduce the resonance factor

$$d = [1 - \rho_0\rho_1 \exp(2i\phi)]^{-1}\,. \tag{4.5}$$

The power gain g_{FP} inside the cavity is given by

$$g_{\mathrm{FP}} = |\tau_0 d|^2. \tag{4.6}$$

The three-port coupler used in reference [4.1] can be represented by the following scattering matrix

$$\mathbf{S_{3p}} = \begin{pmatrix} \eta_2 \exp(i\phi_2) & \eta_1 \exp(i\phi_1) & \eta_0 \exp(i\phi_0) \\ \eta_1 \exp(i\phi_1) & \rho_0 \exp(i\phi_0) & \eta_1 \exp(i\phi_1) \\ \eta_0 \exp(i\phi_0) & \eta_1 \exp(i\phi_1) & \eta_2 \exp(i\phi_2) \end{pmatrix}. \tag{4.7}$$

As stated above, the grating is assumed to be symmetrical with respect to the grating normal. The grating period and the wavelength of light are chosen such that that for normal incidence only the zeroth- and first-order diffraction are present. The magnitudes of their amplitude reflection coefficients are denoted with ρ_0 and η_1 respectively. For incidence at the second order Littrow angle the zeroth, first, and second diffraction orders are present with the magnitudes of the reflection coefficients η_0, η_1, and η_2 as depicted in Fig. 4.1. From the unitarity condition of $\mathbf{S}$ we find the energy conservation law

$$\rho_0^2 + 2\eta_1^2 = 1\,, \tag{4.8}$$

$$\eta_0^2 + \eta_1^2 + \eta_2^2 = 1\,. \tag{4.9}$$

We denote the phase shift associated with the zeroth, first, and second diffraction

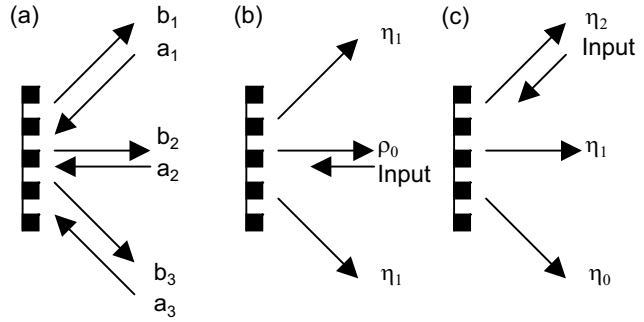

Figure 4.1: Three-port reflection grating: (a) labelling of the input and output ports, (b) amplitudes of reflection coefficients for normal incidence, (c) amplitudes of reflection coefficients for second-order Littrow incidence.

orders as ϕ_0, ϕ_1, and ϕ_2, respectively. As for the mirrors, the values of the phases are not unique. Reflection from a mirror is equivalent to zeroth-order diffraction of a grating. In analogy to the right-hand matrix of equation (4.2) we demand no phase shift for zeroth-order diffraction and therefore set $\phi_0 = 0$. From the unitarity requirement of $\mathbf{S}$ the remaining phases can be calculated, yielding the following possible set of phases:

$$\phi_0 = 0\,, \tag{4.10}$$

$$\phi_1 = -(1/2)\arccos[(\eta_1^2 - 2\eta_0^2)/(2\rho_0\eta_0)]\,, \tag{4.11}$$

$$\phi_2 = \arccos[-\eta_1^2/(2\eta_2\eta_0)]. \tag{4.12}$$

We emphasize that phases ϕ_1 and ϕ_2 are functions of the diffraction efficiencies and therefore vary depending on the properties of the grating. This contrasts with the properties of mirrors, where the phase shift between transmitted and reflected beams is independent of the transmittance and reflectance coefficients. Since phase ϕ_2 is a real number, the modulus of the argument of the arccos in equation (4.12) must be smaller than or equal to 1 and the following upper and lower limits for η_0 and η_2 for a given reflectivity ρ_0 can be derived:

$$\eta_{0,\substack{\max\\\min}} = \eta_{2,\substack{\max\\\min}} = (1 \pm \rho_0)/2. \tag{4.13}$$

Note that these limits are fundamental in that a reflection grating can only be designed and manufactured with diffraction efficiencies within these boundaries. Equations (4.8) - (4.13) provide a full set of three-port coupling relations.

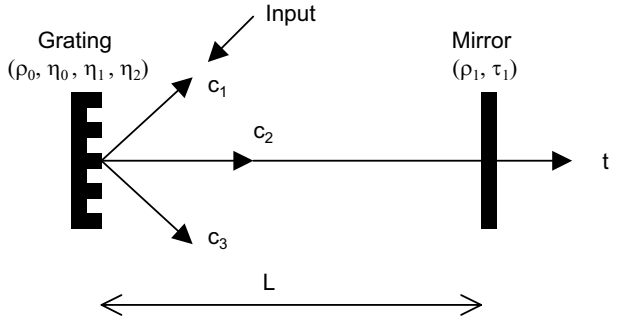

Figure 4.2: Fabry-Perot cavity with a three-port grating coupler and a conventional end mirror. The amplitudes of the fields of interest (c_1, c_2, c_3, t) are indicated by arrows.

Knowledge of the scattering matrix **S** in Eq. (4.7) permits the calculation of input-output relations of interferometric topologies. Here we consider a three-port grating coupled Fabry-Perot cavity. The grating cavity is formed by placing a mirror with amplitude reflectivity ρ_1 at a distance L parallel to the grating surface as is illustrated in Fig. 4.2. To characterize the cavity, the amplitudes c_1, c_3 for the two waves reflected from the cavity and the intracavity amplitude c_2 are calculated as a function of the

cavity length. Assuming unity input and no input at port 3, the cavity is described by

$$\begin{pmatrix} c_1 \\ c_2 \\ c_3 \end{pmatrix} = \mathbf{S_{3p}} \times \begin{pmatrix} 1 \\ \rho_1 c_2 \exp(2i\phi) \\ 0 \end{pmatrix}. \tag{4.14}$$

Solving for the amplitudes yields

$$c_1 = \eta_2 \exp(i\phi_2) + \eta_1^2 \exp[2i(\phi_1 + \phi)]d, \tag{4.15}$$

$$c_2 = \eta_1 \exp(i\phi_1)d, \tag{4.16}$$

$$c_3 = \eta_0 + \eta_1^2 \exp[2i(\phi_1 + \phi)]d\,, \tag{4.17}$$

$$t = i\tau_1 c_2 \exp(i\phi)\,. \tag{4.18}$$

where $\phi = \omega L/c$ is the tuning parameter, d is given according to equation (4.5), and t is the amplitude of the light transmitted through the cavity. The light power at the different ports is proportional to the squared moduli of the amplitudes. The power gain inside the cavity is given by $|c_2|^2 = |\eta_1 d|^2$ analogous to equation (4.6) for a conventional cavity. In contrast with the power gain, the power in the two reflecting ports $|c_1|^2$ and $|c_3|^2$ depends on η_2 and η_0. Figure 4.3 illustrates how the power out

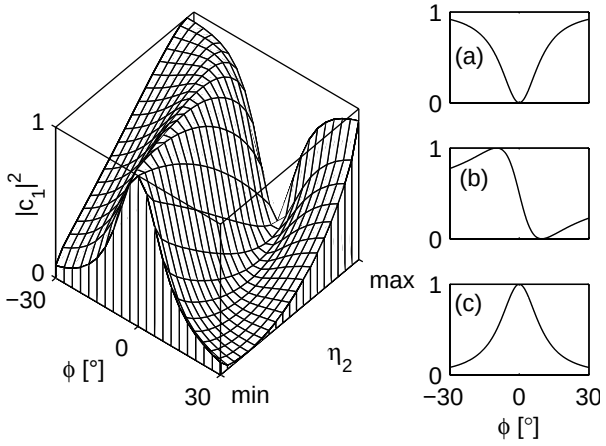

Figure 4.3: Power $|c_1|^2$ of cavity backreflecting port for gratings of different values of η_2. Left, power as a function of ϕ and η_2, right, power as a function of ϕ for (a) $\eta_2 = \eta_{2,\max}$, (b) $\eta_2 = [(\eta_{2,\max}^2 + \eta_{2,\min}^2)/2]^{1/2}$, (c) $\eta_2 = \eta_{2,\min}$. Cavity parameters: $\rho_0^2 = 0.5$, $\rho_1 = 1$.

of the backreflecting port varies as a function of η_2 and the tuning ϕ of the cavity.

For simplicity a cavity with a perfect end mirror $\rho_1 = 1$ is assumed. For a coupler with $\eta_2 = \eta_{2,\max}$, the cavity does not reflect any light back to the laser for a tuning of $\phi = 0$. This corresponds to an impedance-matched cavity that transmits all the light on resonance. For a coupler with $\eta_{2,\min}$, the situation is reversed and all the light is reflected back to the laser. For all other values of η_2 the backreflected intensity has intermediate values and is significantly different from conventional cavities: the intensity as a function of cavity tuning is no longer symmetric to the $\phi = 0$ axis.

Finally, we investigate the influence of loss in the cavity for a coupler with $\eta_{2,\min}$. Figure 4.4 illustrates the effect of an end mirror with transmittance $\tau_1 > 0$ on the power of the two reflecting ports of the cavity on resonance. As a result, apart from the intracavity field, losses affect mainly the back-reflecting port (dotted-dashed curve). The effect on the dark port (solid curve) is minor, as it stays essentially dark as long as the loss τ_1^2 is small compared with the coupling η_1^2.

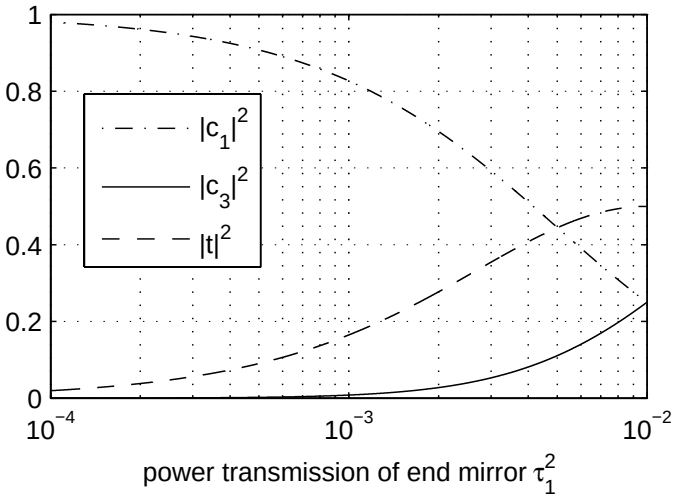

Figure 4.4: Powers of the two reflected ports and the transmitting port as a function of end mirror transmittance τ_1^2 for a coupler with $\rho_0^2 = 0.99$ and $\eta_2 = \eta_{2,\min}$ for a tuning of $\phi = 0$.

In conclusion, we have investigated a three-port reflection grating and derived its coupling relations. A three-port device can be used to couple light into a Fabry-Perot cavity. The input output relations of such a three-port coupled cavity have revealed substantial differences from a conventional cavity. A grating with minimal

η_2 is suitable for a coupler to an arm cavity (single-ended cavity) of a gravitational-wave Michelson interferometer. On resonance all power is reflected back to the beam splitter of the interferometer. Hence no power is lost to the additional port. This makes possible power recycling that is used in all first- and probably also in second- and third-generation detectors. Furthermore we can calculate the phase signals carried by the fields in Eqs. (4.15) and (4.17) when cavity length L is changed and find that the additional port splits a cavity strain signal. However, the complete strain signal is still accessible to detection.

We thank P. Beyersdorf, T. Clausnitzer, E.-B. Kley, R. Schilling, and B. Willke for helpful discussions.

References

[4.1] A. Bunkowksi, O. Burmeister, P. Beyersdorf, K. Danzmann, R. Schnabel, T. Clausnitzer, E.-B. Kley, and A. Tünnermann, *Low-loss grating for coupling to a high-finesse cavity,* Opt. Lett. **29**, 2342 (2004).

[4.2] R. W. P. Drever, *Concepts for Extending the Ultimate Sensitivity of Interferometric Gravitational Wave Detectors Using Non-Transmissive Optics with Diffractive or Holographic Coupling,* in Proceedings of the Seventh Marcel Grossman Meeting on General Relativity, M. Keiser and R.T. Jantzen (eds.), World Scientific, Singapore (1995).

[4.3] S. Rowan, R. Byer, M. Fejer, R. Route, G. Cagnoli, D. Crooks, J. Hough, P. Sneddon, W. Winkler, *Test mass materials for a new generation of gravitational wave detectors,* Proc. of SPIE **4856**, 292 (2003).

[4.4] K.-X. Sun and R.L. Byer, *All-reflective Michelson, Sagnac, and Fabry-Perot interferometers based on grating beam splitters,* Opt. Lett. **23**, 567 (1997).

[4.5] A. Siegman, *Lasers* University Science Books, Sausalito (1986).

Chapter 5

Demonstration of three-port grating phase relations

We experimentally demonstrate the phase relations of three-port gratings by investigating three-port coupled Fabry-Perot cavities. Two different gratings that have the same first-order diffraction efficiency but differ substantially in their second-order diffraction efficiency have been designed and manufactured. Using the gratings as couplers to Fabry-Perot cavities, we could validate the results of an earlier theoretical description of the phases at a three-port grating [Opt. Lett. **30**, 1183 (2005)].

Originally published as A. Bunkowski et al., Opt. Lett. **31**, 2384 (2006).

Conventional interferometers rely on splitting and recombining optical fields with partly transmissive beam splitters. When transmission through optical substrates is disadvantageous, diffractive reflection gratings can also serve as beam splitters, allowing for all-reflective interferometry [5.1]. As long as the grating splits an incoming beam into two outgoing beams, the phase relation at the grating, and hence the properties of the interferometer built thereof, are analogous to the well-known ones of a transmissive two-port beam splitter. However, if a diffractive beam splitter has more than two orders, the mirror analog, and thus the simple phase relation, no longer hold. Still, a knowledge of these relations at the diffractive beam splitter is essential for an understanding of multiple-port interferometry. In a recent experiment, a grating in a

second-order Littrow mount was used to couple light into a Fabry-Perot cavity [5.2]. In this case, the incoming beam was split into three outgoing beams. The phase relations at the so-called three-port grating were analyzed theoretically and the input-output relations for a Fabry-Perot cavity with a three-port coupler were derived [5.3]. The theoretical investigation of the phases was based solely on energy conservation and reciprocity of the device, but there has not yet been an experimental validation of the results.

In this Letter we report an experiment that was performed to demonstrate the phase relations of optical three-port devices. Two different gratings were designed and manufactured for this purpose, and used as couplers to Fabry-Perot interferometers.

Phase relations for three-port gratings with equal diffraction efficiencies in the $\pm$ first orders can be written as [5.3, 5.4]

$$\phi_0 = 0\,, \tag{5.1}$$

$$\phi_1 = -(1/2)\arccos[(\eta_1^2 - 2\eta_0^2)/(2\rho_0\eta_0)]\,, \tag{5.2}$$

$$\phi_2 = \arccos[-\eta_1^2/(2\eta_2\eta_0)]\,, \tag{5.3}$$

where ϕ_0, ϕ_1, and ϕ_2 are the phase shifts for zeroth, first, and second diffraction orders, respectively. Interestingly, the coupling phases depend on the coupling amplitudes,

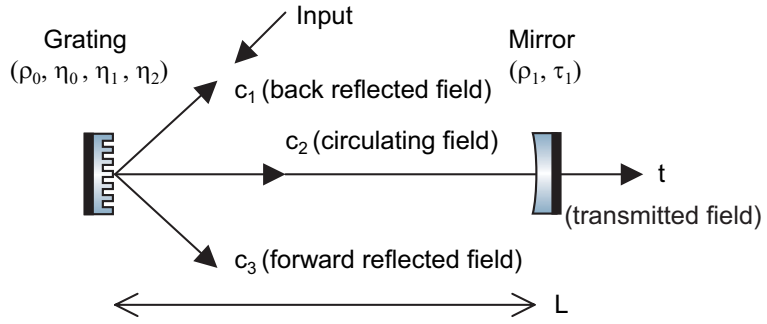

Figure 5.1: Grating in second-order Littrow mount with naming convention given in the text.

which are given by η_0, η_1, and η_2 for the zeroth, first, and second-diffraction orders, respectively, and by ρ_0 for the normal incidence reflectivity of the grating.

Direct measurements of beam splitter phase relations are difficult. However, if the three-port beam splitter is used to couple light into a cavity, the cavity properties

can be used to validate the phase relations. Figure 5.1 shows the optical layout of a Fabry-Perot interferometer with a three-port grating coupler. The grating is used in a second-order Littrow mount, and light from a laser source is coupled to the interferometer via the grating's first order. The field amplitudes of the back-reflected light (c_1) and forward-reflected light (c_3) result from interference of the input field with the intracavity field and directly depend on the phase relations between the grating ports. In Ref. [5.3], amplitude reflection coefficients for c_1 and c_3, as well as the amplitudes for the intra-cavity field (c_2) and the transmitted field (t), were derived and are repeated here for convenience.

$$c_1 = \eta_2 \exp(i\phi_2) + \eta_1^2 \exp[2i(\phi_1 + \phi)]d\,, \tag{5.4}$$

$$c_2 = \eta_1 \exp(i\phi_1)d\,, \tag{5.5}$$

$$c_3 = \eta_0 + \eta_1^2 \exp[2i(\phi_1 + \phi)]d\,, \tag{5.6}$$

$$t = i\tau_1 c_2 \exp(i\phi)\,, \tag{5.7}$$

where the amplitude reflectance and transmittance of the cavity end mirror are given by ρ_1 and τ_1, respectively. The resonance factor is given by $d = [1 - \rho_0\rho_1 \exp(2i\phi)]^{-1}$, and the length L of the cavity is expressed by the tuning parameter $\phi = \omega L/c$, where ω is the angular frequency and c the speed of light.

One distinct feature of this type of grating cavity is that the grating phase relations allow for reflection coefficients (as a function of ϕ) that are not symmetric to the detuning of the cavity. Figure 5.2 shows the calculated power back reflectance $|c_1|^2$ of a cavity with input coupling of $\eta_1^2 = 0.1$ and an ideal end mirror ($\rho_1 = 1$) as a function of cavity tuning ϕ for selected values of the second-order diffraction efficiency η_2^2. In all cases shown, the cavity finesse is the same. For an ideal (lossless) grating, the finesse depends on the first order diffraction efficiency $\eta_1 = [(1-\rho_0)/2]^{1/2}$ only. For the minimal second-order diffraction efficiency [5.3] $\eta_{2,\mathrm{min}} = (1 - \rho_0)/2$, all the light is reflected back towards the laser source if the cavity is on resonance ($\phi = 0 \mod \pi$). However, for maximal second-order diffraction efficiency $\eta_{2,\mathrm{max}} = (1+\rho_0)/2$, no light is reflected back from a resonating cavity. Hence for the extremal values of η_2 the back-reflected port behaves either exactly like the reflection port or the transmission port of a conventional, impedance-matched, two-mirror Fabry-Perot cavity. For intermediate values of η_2, the power reflectance is no longer symmetric to the $\phi = 0$ axis, and the

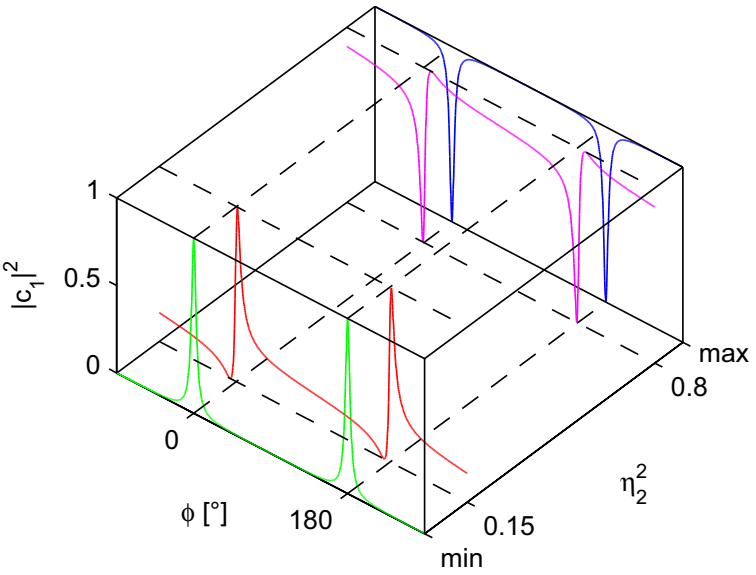

Figure 5.2: Calculated power back reflectance $|c_1|^2$ for a cavity with coupling $\eta_1^2 = 0.1$ and an end mirror with $\rho_1 = 1$ as a function of cavity tuning (ϕ) for selected values of second-order diffraction efficiency η_2^2.

resonance peaks are not of the usual Airy form, as can be seen for the two exemplary curves, $\eta_2^2 = 0.15$ and $\eta_2^2 = 0.8$, in Figure 5.2.

To verify the grating behavior, two gratings with essentially the same first-order diffraction efficiency but substantially different second- and hence zeroth-order diffraction efficiency were designed and manufactured. The gratings use a binary structure written into the top layer of a dielectric multilayer stack consisting of Ta_2O_5 and SiO_2 placed on a fused silica substrate. We chose a grating period of $p = 1450\,\text{nm}$, which corresponds to a second-order Littrow angle of 47.2° for the Nd:YAG laser wavelength of 1064 nm used. A rigorous coupled wave analysis [5.5] was performed to design the grating. The ridge width is $p/2$, and the top layer consists of 880 nm of SiO_2. Figure 5.3 shows the calculated diffraction efficiencies for all three diffraction orders in the second-order Littrow mount as a function of groove depth. The gratings were produced by ultrafast high-accuracy electron beam direct writing [5.6] (electron beam writer ZBA23h from Leica Microsystems Jena GmbH) and etched by means of reactive ion beam etching. The etching process was stopped after reaching a groove depth of

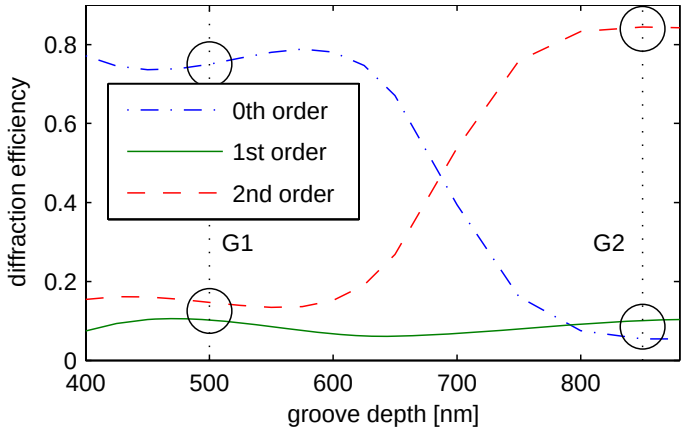

Figure 5.3: (Calculated diffraction efficiencies as a function of groove depth obtained with RCW calculations for the gratings used. The circles show the design values of our gratings G1 and G2, respectively.

500 nm (G1) and 850 nm (G2), respectively.

A sketch of the experimental setup used to verify the grating phase relations is shown in Fig. 5.4. A beam of a diode-pumped Nd:YAG non-planar ring oscillator (Model Mephisto from Innolight GmbH) was spatially filtered with a triangular ring cavity. The grating (either G1 or G2) was illuminated at a second-order Littrow angle, and a cavity end mirror with $\tau_1^2 = 300$ parts per million was placed parallel to the grating's surface. The cavity length could be controlled by a piezoelectric transducer, and the three ports of interest were monitored by photodetectors.

Figures 5.5 and 5.6 show the measured signals from the three photodetectors for linear cavity scans over one free spectral range using G1 and G2, respectively. Also shown are the theoretical curves $|c_1(\phi)|^2$, $|c_3(\phi)|^2$, and $|t(\phi)|^2$, which were obtained from Eqs. (5.4), (5.6), and (5.7) using measured efficiencies of the two gratings. Coupling to the cavity was measured to be identical for both gratings within the measurement accuracy of about 5 % of the power meter used, $\eta_1^2(\mathrm{G1}) = \eta_1^2(\mathrm{G2}) = 0.10$. For the first grating, a value of $\eta_2^2(\mathrm{G1}) = 0.15$ was measured, and for the second one, a value of $\eta_0^2(\mathrm{G2}) = 0.10$ was measured. The remaining values were calculated using the identities $\eta_0^2 + \eta_1^2 + \eta_2^2 = 1$ and $\rho_0^2 + 2\eta_1^2 = 1$. We found the calculated values within the error bars of direct measurements.

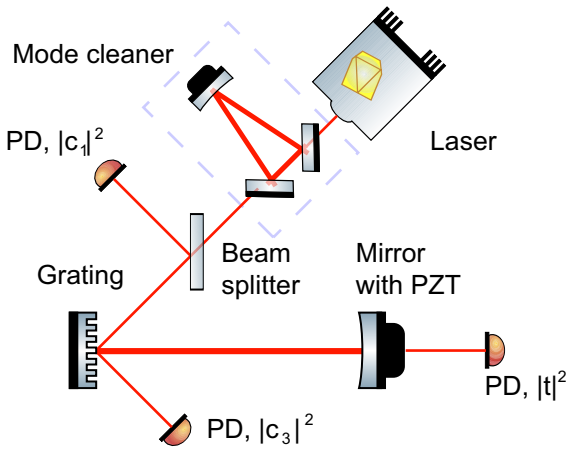

Figure 5.4: Experimental setup: PZT, piezoelectric transducer; PD, photodetector.

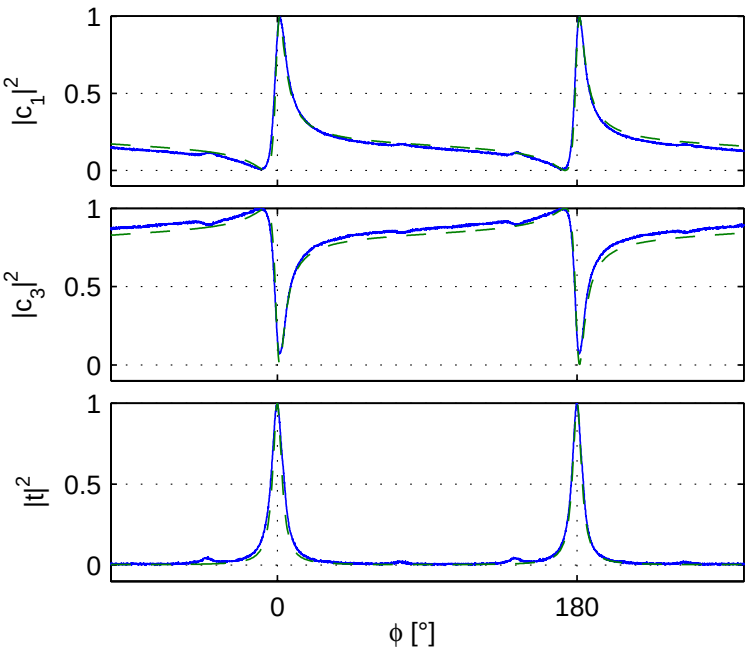

Figure 5.5: (Normalized powers at the three photo detectors for three-port coupler G1 as the cavity length was linearly scanned (solid, blue curve) and the calculated values (dashed-dotted, green curve).

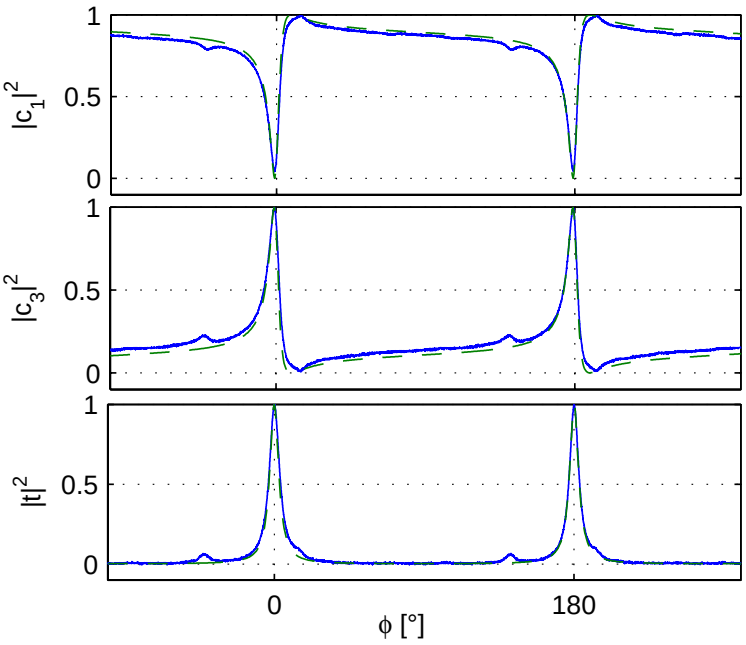

Figure 5.6: Normalized powers at the three photo detectors for three-port coupler G2 as the cavity length was linearly scanned (solid, blue line) and the calculated values (dashed, green curve).

Figures 5.5 and 5.6 show that the theoretical and measured curves agree very well. The interference at the three-port gratings could therefore be well described by the phase relations according to Eqs. (5.1)-(5.3). The small deviations are possibly due to imperfect mode matching, and losses at the grating that may be caused by transmission, scattering, and diffraction from periodic grating errors. As predicted, the measured intensities in the reflecting ports showed the asymmetric behavior around cavity resonances.

In conclusion, we have designed and manufactured two diffraction gratings that allowed the construction of grating-coupled Fabry-Perot cavities with the same finesse but with totally different properties of the two reflected ports, thereby confirming the phase relations that were earlier derived theoretically. Our experimental results could be fully described by phase relations based on energy conservation and reciprocity and the knowledge of the grating's diffraction efficiencies. No further information about

the gratings was required.

This research was supported by the Deutsche Forschungsgemeinschaft within the Sonderforschungsbereich TR7.

References

[5.1] K.-X. Sun and R. L. Byer, *All-reflective Michelson, Sagnac, and Fabry-Perot interferometers based on grating beam splitters,* Opt. Lett. **23**, 567 (1997).

[5.2] A. Bunkowksi, O. Burmeister, P. Beyersdorf, K. Danzmann, R. Schnabel, T. Clausnitzer, E.-B. Kley, and A. Tünnermann, *Low-loss grating for coupling to a high-finesse cavity,* Opt. Lett. **29**, 2342 (2004).

[5.3] A. Bunkowski, O. Burmeister, K. Danzmann, and R. Schnabel, *Input-output relations for a three-port grating coupled Fabry-Perot cavity,* Opt. Lett. **30**, 1183 (2005).

[5.4] R. Schnabel, A. Bunkowski, O. Burmeister, and K. Danzmann, *Three-port beam splitters-combiners for interferometer applications,* Opt. Lett. **31**, 658 (2006).

[5.5] M. G. Moharam, and T. K. Gaylord, *Diffraction analysis of dielectric surface-relief gratings,* J. Opt. Soc. Am. **72**, 1385 (1982).

[5.6] E.-B. Kley, T. Clausnitzer, M. Cumme, K. Zöllner, B. Schnabel, *Investigation of large area gratings fabricated by ultrafast e-beam writing* in *Advanced Optical Manufacturing and Testing Technology*, Proc. SPIE **4231**, 116 (2000).

Chapter 6

Three-port beam splitters-combiners for interferometer applications

We derive generic phase and amplitude coupling relations for beam splitters-combiners that couple a single port with three output ports or input ports, respectively. We apply the coupling relations to a reflection grating that serves as a coupler to a single-ended Fabry-Perot ring cavity. In the impedance-matched case such an interferometer can act as an all-reflective ring mode cleaner. It is further shown that in the highly undercoupled case almost complete separation of carrier power and phase signal from a cavity strain can be achieved.

Originally published as R. Schnabel, A. Bunkowski, O. Burmeister, and K. Danzmann, Opt. Lett. **31**, 658 (2006).

Two-port beam splitters-combiners, for example, the partially transmitting mirror, are key devices in laser interferometry. They serve as 50/50 beam splitters in Michelson interferometers and as low transmission couplers to cavities. Amplitude and phase relations of two-port beam splitters-combiners are well known. In the case of grating optics, diffraction orders of a greater number can couple to one input port. Recently a reflection grating with three diffraction orders was used for interferometer purposes;

laser light was coupled into a linear high-finesse Fabry-Perot cavity by using the second-order Littrow configuration [6.1]. The grating was built from a binary structure. This property, together with the second-order Littrow configuration, provided a symmetry against the grating's normal. The system was theoretically analyzed in Ref. [6.2]. It was shown that a new three-port (3p) coupled Fabry-Perot interferometer can be designed such that resonating carrier light is completely backreflected towards the laser source. The additional interferometer port is then on a dark fringe and contains half of the interferometer strain signal.

In this letter we first derive the generic coupling relations of 3p beam splitters. This includes coupling amplitudes and coupling phases that are required for interferometric applications. Our description includes arbitrary gratings with three orders of diffraction regardless of the groove shape and the diffraction angles, as shown in Fig. 6.1. We then investigate the 3p reflection grating coupled Fabry-Perot ring interferometer and show that for a resonating carrier a dark port can be constructed that contains an arbitrary high fraction of the interferometer's strain signal.

Optical devices can be described by a scattering matrix formalism [6.3]. In general the coupling of n input and n output ports requires an $n \times n$ scattering matrix $\mathbf{S}$. The n complex amplitudes of incoming and outgoing fields are combined into vectors $\mathbf{a}$ and $\mathbf{b}$, respectively. For a lossless device $\mathbf{S}$ has to be unitary to preserve energy, and reciprocity demands $|S_{ij}| \equiv |S_{ji}|$ for all elements S_{ij} of $\mathbf{S}$. For a generic 3p device six coupling amplitudes and nine coupling phases are involved. Since three input and three output fields are considered, the number of phases can be reduced to six without loss of physical generality; the remaining six phases describe the phases of the six fields with respect to a local oscillator field. Here we choose the phases such that the matrix $\mathbf{S}$ is symmetric, and $\mathbf{b} = \mathbf{S} \times \mathbf{a}$ can therefore be written as

$$\begin{pmatrix} b_1 \\ b_2 \\ b_3 \end{pmatrix} = \begin{pmatrix} \eta_1 e^{i\phi_1} & \eta_4 e^{i\phi_4} & \eta_5 e^{i\phi_5} \\ \eta_4 e^{i\phi_4} & \eta_2 e^{i\phi_2} & \eta_6 e^{i\phi_6} \\ \eta_5 e^{i\phi_5} & \eta_6 e^{i\phi_6} & \eta_3 e^{i\phi_3} \end{pmatrix} \times \begin{pmatrix} a_1 \\ a_2 \\ a_3 \end{pmatrix}, \tag{6.1}$$

where $0 < \eta_i < 1$ for all i describes the amplitude and $e^{i\phi_i}$ describes the phase of coupling. Figure 6.1 shows two examples of 3p devices. In both cases the input beam splits into three beams, and, vice versa, three input beams can interfere to become a

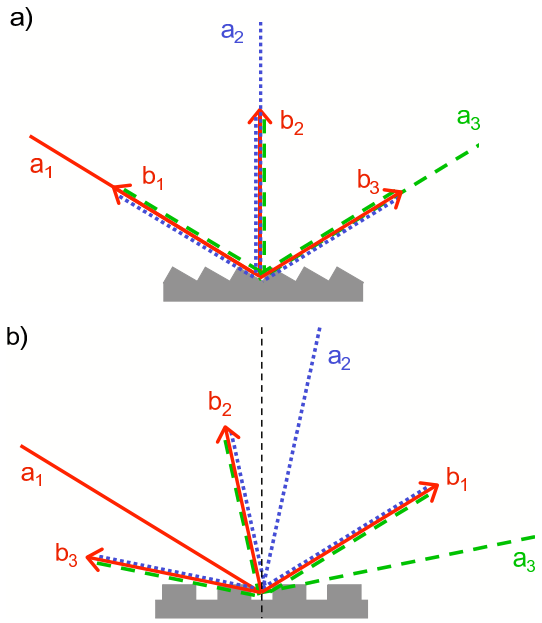

Figure 6.1: Two examples of three-port (3p) beam splitters and/or combiners. Input fields a_i and output fields b_i denote complex amplitudes of the electric field. (a) Asymmetric triangular grating in second-order Littrow configuration. (b) Binary grating in non-Littrow configuration.

single one. However, one realizes that the rigourously defined scattering matrix for the device in Fig. 6.1(b) has a dimension of 6×6, but this matrix contains null elements because not six but only three ports couple, and the matrix can be reduced to the matrix as given in Eq. (6.1).

The unitarity condition $\mathbf{S}^\dagger\mathbf{S} = \mathbf{1}$ entails the following set of equations:

$$1 = \eta_1^2 + \eta_4^2 + \eta_5^2\,, \tag{6.2}$$

$$1 = \eta_2^2 + \eta_4^2 + \eta_6^2\,, \tag{6.3}$$

$$1 = \eta_3^2 + \eta_5^2 + \eta_6^2\,, \tag{6.4}$$

$$|\cos(2\phi_4 - \phi_1 - \phi_2)| = \frac{|\eta_5^2\eta_6^2 - \eta_1^2\eta_4^2 - \eta_2^2\eta_4^2|}{2\eta_4^2\eta_1\eta_2}\,, \tag{6.5}$$

$$|\cos(2\phi_5 - \phi_1 - \phi_3)| = \frac{|\eta_4^2\eta_6^2 - \eta_1^2\eta_5^2 - \eta_3^2\eta_5^2|}{2\eta_5^2\eta_1\eta_3}\,, \tag{6.6}$$

$$|\cos(2\phi_6 - \phi_2 - \phi_3)| = \frac{|\eta_4^2\eta_5^2 - \eta_2^2\eta_6^2 - \eta_3^2\eta_6^2|}{2\eta_6^2\eta_2\eta_3}\,, \tag{6.7}$$

$$|\cos(\phi_6 + \phi_4 - \phi_5 - \phi_2)| = \frac{|\eta_1^2\eta_4^2 - \eta_2^2\eta_4^2 - \eta_5^2\eta_6^2|}{2\eta_2\eta_4\eta_5\eta_6}\,, \tag{6.8}$$

$$|\cos(\phi_6 - \phi_4 - \phi_5 + \phi_1)| = \frac{|\eta_3^2\eta_5^2 - \eta_1^2\eta_5^2 - \eta_4^2\eta_6^2|}{2\eta_1\eta_4\eta_5\eta_6}\,, \tag{6.9}$$

$$|\cos(\phi_6 - \phi_4 + \phi_5 - \phi_3)| = \frac{|\eta_2^2\eta_6^2 - \eta_4^2\eta_5^2 - \eta_3^2\eta_6^2|}{2\eta_3\eta_4\eta_5\eta_6}\,. \tag{6.10}$$

Equations (6.2)-(6.10) set boundaries for physically possible coupling amplitudes and phases of the generic lossless 3p beam splitter-combiner. Equations (6.2)-(6.4) represent the energy conservation law and arise from the diagonal elements of the unitarity condition. Equations (6.5)-(6.10) arise from the off-diagonal elements. They are already simplified to contain just a single cosine term. However, it can be easily deduced that up to three phases in the scattering matrix $\mathbf{S}$ can be chosen arbitrarily. In this analysis we choose the phases ϕ_1, ϕ_2, ϕ_3 to be zero. This is a permitted choice without introducing any restriction on possible coupling amplitudes. Then the phases of the scattering matrix can be written as

$$\begin{aligned}
\phi_1 &= \phi_2 = \phi_3 = 0\,,\\
\phi_4 &= -\frac{1}{2}\arccos\left(\frac{\eta_1^2\eta_4^2 + \eta_2^2\eta_4^2 - \eta_5^2\eta_6^2}{2\eta_4^2\eta_1\eta_2}\right) - \frac{\pi}{2}\,,\\
\phi_5 &= \frac{1}{2}\arccos\left(\frac{\eta_4^2\eta_6^2 - \eta_1^2\eta_5^2 - \eta_3^2\eta_5^2}{2\eta_5^2\eta_1\eta_3}\right)\,,\\
\phi_6 &= -\frac{1}{2}\arccos\left(\frac{\eta_2^2\eta_6^2 + \eta_3^2\eta_6^2 - \eta_4^2\eta_5^2}{2\eta_6^2\eta_2\eta_3}\right) + \frac{\pi}{2}\,.
\end{aligned} \tag{6.11}$$

It is interesting to note that the coupling relations restrict the possible values of η_i. Let us assume that a free choice of η_4^2 and η_6^2 is desired, which then immediately determines η_2^2 according to Eq. (6.3). Substituting η_1 and η_3 by using Eqs. (6.2) and

(6.4), Eqs. (6.5)-(6.10) provide the following pair of inequalities that restricts the values of η_5 and thereby also the values of η_1 and η_3:

$$\frac{\eta_4\eta_6\,(1-\eta_2)}{\eta_4^2+\eta_6^2} \leq \eta_5 \leq \frac{\eta_4\eta_6\,(1+\eta_2)}{\eta_4^2+\eta_6^2}\,. \tag{6.12}$$

We now apply a 3p beam splitter-combiner in interferometry. We focus on the device in figure 6.1(b) as a coupler to a Fabry-Perot ring cavity as shown in Fig. 6.2. Laser light incident from the left is coupled according to η_4^2 into the cavity, which is formed by the grating and two additional highly reflecting cavity mirrors. If both cavity mirrors are lossless, the cavity finesse depends on the specular reflectivity η_2^2 and does not rely on high values of first- or second-order diffraction efficiencies. Using high reflection dielectric coatings makes high-finesse values and high laser buildups possible, similar to the linear cavity investigated in reference [6.1]. However, here the cavity outputs depend on η_4^2 (into port c_1) and η_6^2 (into port c_3) that can have different values.

Assuming unity laser input and perfectly reflecting cavity mirrors, the system is described by

$$\begin{pmatrix} c_1 \\ c_2 \\ c_3 \end{pmatrix} = \mathbf{S}\times \begin{pmatrix} 1 \\ c_2\exp(2i\theta) \\ 0 \end{pmatrix}. \tag{6.13}$$

Here $\theta = \omega L/c$ denotes the detuning from cavity resonance, with L the cavity length, ω the laser field angular frequency and c the speed of light. Solving for the reflected amplitudes yields

$$c_1 = \eta_1 + \frac{\eta_4^2\exp[2i(\phi_4+\theta)]}{1-\eta_2\exp(2i\theta)} \tag{6.14}$$

$$c_2 = \frac{\eta_4\exp(i\phi_4)}{1-\eta_2\exp(2i\theta)} \tag{6.15}$$

$$c_3 = \eta_5\exp(i\phi_5) + \frac{\eta_4\eta_6\exp[i(\phi_4+\phi_6+2\theta)]}{1-\eta_2\exp(2i\theta)} \tag{6.16}$$

From Eq. (6.14) it can be shown that, for a grating with η_5^2 at its maximum value for given η_4^2 and η_6^2, and a cavity on resonance ($\theta = 0$), no carrier light from the laser incidenting from the left is leaving the cavity to the left ($c_3 = 0$). This dark port is

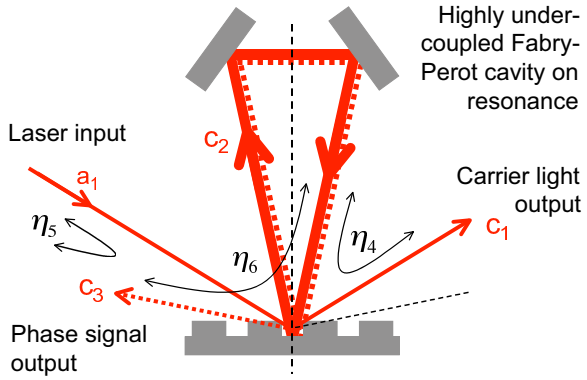

Figure 6.2: Three-port coupled grating in a ring Fabry-Perot interferometer. The grating can be designed such that the laser input is completely sent into port c_1 on cavity resonance. If the cavity is impedance matched this device might serve as an all-reflective mode cleaner. Another interesting case occurs in which the cavity is highly undercoupled. Then almost the complete cavity strain signals are send to port c_3. Such a device separates carrier light from its modulation sidebands.

indicated in Fig. 6.2 by a dashed arrow. If the cavity moves away from resonance, for example, caused by a cavity strain, amplitude c_3 is no longer zero. This field is generally termed a phase signal and might appear at some sideband frequency Ω if the cavity is locked to the time-averaged carrier frequency ω_0 with locking-bandwidth smaller than Ω. The phase signal generated inside the cavity obviously leaves the cavity according to the magnitudes of η_4^2 and η_6^2 in two directions. From Eqs. (6.14) and (6.16) it is easy to prove that the power of the signal indeed splits according to the ratio η_4^2/η_6^2. We now discuss two distinct examples; in both of them we consider η_5^2 to be designed close to its maximum value. For $\eta_4^2 = \eta_6^2$ the cavity output coupling is twice the input coupling and the signal is split into two equal halves. We term this case a symmetric or an impedance-matched 3p coupled cavity; this is in analogy to the lossless impedance-matched linear cavity whose output coupling is also twice the input coupling. However, due to the choice of η_5^2 all the carrier power is sent into port c_1 if the cavity is on resonance as discussed above. Such a device can serve as an all-reflective mode cleaner. For $\eta_4 > \eta_6$ the 3p coupled lossless cavity can be termed overcoupled and for $\eta_4 < \eta_6$ undercoupled. As the second example we consider the highly undercoupled grating cavity ($\eta_4^2 \ll \eta_6^2 \ll \eta_2^2$) and explicitly choose the following

coupling coefficients:

$$\begin{array}{lll} \eta_4^2 = 0.0001\,, & \eta_6^2 = 0.0099\,, & \eta_2^2 = 0.99\,, \\ \eta_5^2 = 0.0394\,, & \eta_1^2 = 0.9605\,, & \eta_3^2 = 0.9507\,, \\ \phi_1 = 0\,, & \phi_2 = 0\,, & \phi_3 = 0\,, \\ \phi_4 \approx -3.1349\,, & \phi_5 \approx 1.5708\,, & \phi_6 \approx 1.5707\,. \end{array} \tag{6.17}$$

For this set of measures again η_5^2 is almost at its maximum value, and consequently η_1^2 and η_3^2 are close to their minimum values. As in the impedance-matched case described above, again all the carrier power is sent into port c_1. Owing to the high asymmetry of the ratio between η_4^2 and η_6^2 the *signal* is sent mainly into port c_3. The special property of the highly undercoupled grating Fabry-Perot interferometer is therefore the possibility of separating carrier light and phase signal. This is a remarkable result. Separation of carrier light and phase signal is well known for a Michelson interferometer operating on a dark fringe. Such an interferometer sends all the laser power back to the laser source. The antisymmetric mode of phase shifts in the Michelson arms is sent into the dark port. The symmetric mode is combined with the reflected laser power and sent toward the bright port. In case of the highly undercoupled 3p grating Fabry-Perot interferometer the almost complete phase signal is separated from carrier light and is accessible to detection, and the reflected field in the bright port contains only a marginal fraction of the signal (η_4^2/η_6^2).

We point out that all results obtained for the Fabry-Perot ring interferometer using the 3p coupler in Fig. 6.1(b) also hold for a linear cavity using the 3p coupler in Fig. 6.1(a). However, some distinctive properties should be mentioned. Regardless of their different topologies, the ring Fabry-Perot interferometer is content with only low efficiencies for greater than zero diffraction orders. All coupling amplitudes in Eqs. (6.17) with values close to unity describe specular reflections. The production of such a grating with low overall loss should be possible with standard technologies building on the concept used in Refs. [6.1] and [6.4]. In case of the (highly undercoupled) linear Fabry-Perot interferometer η_1^2 and η_3^2 do not describe specular reflections, and high diffraction efficiencies in the second-order diffraction are required. However, especially in the second order Littrow configuration, carrier and signal separation offers straightforward extension by interferometer recycling techniques [6.5].

This work was supported by the Deutsche Forschungsgemeinschaft within the Sonderforschungsbereich TR7.

References

[6.1] A. Bunkowski, O. Burmeister, P. Beyersdorf, K. Danzmann, R. Schnabel, T. Clausnitzer, E.-B. Kley, and A. Tünnermann, *Low-loss grating for coupling to a high-finesse cavity,* Opt. Lett. **29**, 2342 (2004).

[6.2] A. Bunkowski, O. Burmeister, K. Danzmann, and R. Schnabel, *Input-output relations for a three-port grating coupled Fabry-Perot cavity,* Opt. Lett. **30**, 1183 (2005).

[6.3] A. E. Siegmann, *Lasers* University Science Books, Sausalito (1986).

[6.4] T. Clausnitzer, E.-B. Kley, A. Tünnermann, A. Bunkowski, O. Burmeister, K. Danzmann, R. Schnabel, A. Duparré, and S. Gliech, *Study on ultra low-loss low-efficiency diffraction gratings,* Opt. Exp. **13**, 4370 (2005),

[6.5] G. Heinzel, K. A Strain, J. Mizuno, K. D. Skeldon, B. Willke, W. Winkler, R. Schilling, A. Rüdiger, and K. Danzmann, *Experimental Demonstration of a Suspended Dual Recycling Interferometer for Gravitational Wave Detection,* Phys. Rev. Lett. **81**, 5493 (1998).

Chapter 7

High reflectivity grating waveguide coatings for 1064 nm

We propose thin single-layer grating waveguide structures to be used as high-reflectivity, but low thermal noise, alternative to conventional coatings for gravitational wave detector test mass mirrors. Grating waveguide (GWG) coatings can show a reflectivity of up to 100% with an overall thickness of less than a wavelength. We theoretically investigate GWG coatings for 1064 nm based on tantala (Ta_2O_5) on a Silica substrate focussing on broad spectral response and low thickness.

Originally published as A. Bunkowski et al., Class. Quantum Grav. **23**, 7297 (2006).

7.1 Introduction

Dedicated research during the last few years has revealed that thermally driven motion of the test masses, so-called thermal noise [7.1], is larger than foreseen in future gravitational wave detectors. A major, but previously underestimated, contribution is given by the multilayer dielectric coating stacks of the high reflectivity test mass mirrors [7.2, 7.3]. This currently limits the design sensitivity of the Advanced LIGO detector [7.4]. In conventional schemes, up to 40 layers of Ta_2O_5 and SiO_2 with an optical thickness of a quarter wavelength are needed to reach high reflectivities suffi-

ciently close to 100 %. The thermal noise of the coating is due to the mechanical loss angle of the layers with a dominant contribution from Ta_2O_5. New concepts are required that have less loss but still achieve the required high reflectivity. One approach being pursued is to design an alternative multilayer system deviating from the classical quarter wave design and containing less Ta_2O_5 [7.5]. Doping of Ta_2O_5 with TiO_2 has also been investigated and a reduction of the loss by a factor of 1.5 was observed [7.6]. Another approach is to avoid high reflection coatings at all by the use of corner reflectors which employ total internal reflection instead of multiple interference at different layers to reach high reflectivity [7.7]. However, in this case thermo-refractive noise which results from a temperature dependent refractive index and also thermal lensing are increased due to the large optical path length in the substrate material.

Grating waveguide structures [7.8] provide another possibility to construct high reflectivity devices. The interest of earlier work on grating waveguides lay mainly in narrowband (highly resonant) devices for applications in optical filtering [7.9] and optical switching [7.10]. However, grating waveguide structures can also provide broadband (weakly resonant) reflectors. This makes them interesting candidates for test mass coatings in gravitational wave detectors, because only a very small amount of dielectric coating material is required which results in a considerable reduction in coating thermal noise.

7.2 Resonant grating waveguide structures

The remarkable property of a grating waveguide (GWG) is that it can show a reflectivity of 100 % for a given optical wavelength λ despite its thickness of typically less than a wavelength. For an extensive overview of grating waveguides we refer to [7.11]. In the simplest case a GWG consists of a substrate material with low refractive index n_L followed by a waveguide layer with high refractive index n_H which has periodic corrugation with period d as shown in Figure 7.1. A simplified ray picture [7.8] can be used to understand its behavior. The structure can be designed such that light incident onto the grating will only produce one diffraction order in reflection (0R) but three diffraction orders in transmission (0T and $\pm$1T). (For clarity the -1T order has been omitted in Figure 7.1.)

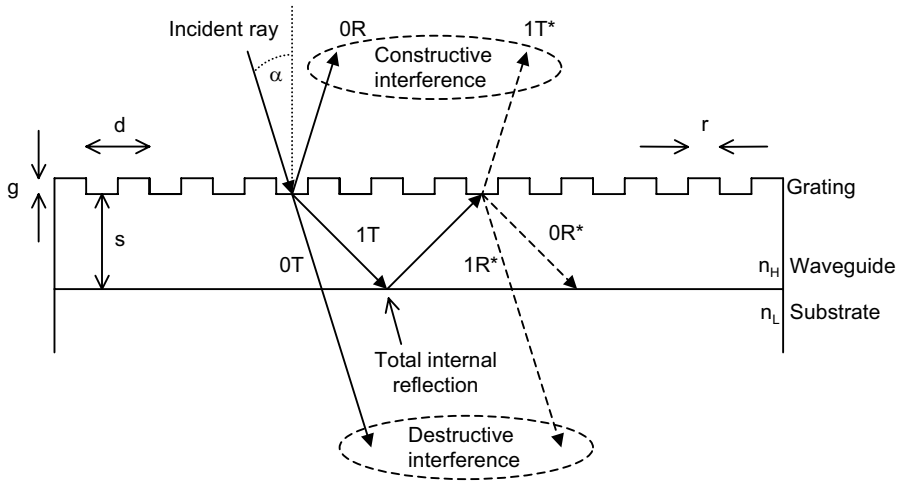

Figure 7.1: Schematic of a grating waveguide structure in a simplified ray picture. For clarity a non zero angle of incidence and only one first order transmission is shown.

The-first order beams are coupled into a layer of high refractive material where they are stored due to total internal reflection. Light inside the waveguide is also coupled out via the grating. For a proper choice of grating parameters and incident angle, the light coupled out from the layer (1R*) interferes destructively with the zero order transmitted beam (0T) and the device is a perfect reflector.

The possible parameter range for the period d depends on the angle of incidence α, the (vacuum) laser wavelength λ (λ_0), and the refractive indices n_L and n_H and can be calculated from the grating equation

$$\sin\alpha + \sin\beta_m = m\lambda/d, \tag{7.1}$$

where β_m is the angle of the mth diffraction order. For test mass mirrors in gravitational wave detector Michelson interferometers the angle of incidence is typically restricted to $\alpha = 0$. To ensure that only the $m = 0$ order is allowed in reflection,

$$d < \lambda_0 \tag{7.2}$$

has to hold. Another condition is that only $|m| \leq 1$ orders in transmission exist from which follows that

$$1 < d\frac{n_\mathrm{H}}{\lambda_0} < 2. \tag{7.3}$$

Total internal reflection of the first order at the boundary of the waveguide and the substrate material is ensured if

$$d < \lambda_0 / n_{\mathrm{L}}. \tag{7.4}$$

A resonant grating waveguide structure has analogous behavior to a Fabry-Perot resonator: with decreasing coupling to the waveguide the finesse of the structure increases [7.8]. For high reflectors in GW detectors high finesse structures are disadvantageous, because small deviations from the design parameter would dramatically decrease the reflectivity for the desired wavelength λ_0. Additionally the power build-up inside a high finesse waveguide could be a problem for high-power laser interferometers. Accordingly, a broadband resonance is desired for the high reflector.

7.3 Spectral response of waveguide coatings

Using Rigorous Coupled Wave (RCW) analysis [7.12] it is possible to calculate the optical properties of the structure. Design considerations for binary gratings must include groove depth g, waveguide thickness s and ridge width r, see Figure 7.1, in addition to the before mentioned period d and refractive indices n_{L} and n_{H}. The goal is to design a broad band reflection being less sensitive to fabrication tolerances and avoiding the problem of strong light power gain in the waveguide. Here we restrict ourselves to $n_{\mathrm{H}} = 2.04$ and $n_{\mathrm{L}} = 1.45$. This corresponds to tantala and fused silica which are the favorite high index coating material and test mass material, respectively [7.2].

According to (7.2) – (7.4) the following constraints apply to the period when one assumes the commonly used Nd:YAG laser wavelength of $\lambda_0 = 1064\,\mathrm{nm}$:

$$521\,\mathrm{nm} < d < 734\,\mathrm{nm}. \tag{7.5}$$

For a broadband response, the coupling to the waveguide which corresponds to the diffraction efficiency of the ± 1T ray should be maximized. It only depends on the grating properties g and r/d but not on the thickness s of the waveguiding layer. Figure 7.2 shows how the coupling depends on the groove depth g and fill factor (r/d) for selected values of d for TM (magnetic field vector is parallel to the grooves) illumination. The plots indicate that the maximum coupling increases with increasing period d. This is illustrated in Figure 7.3 where we plotted the maximum values of the

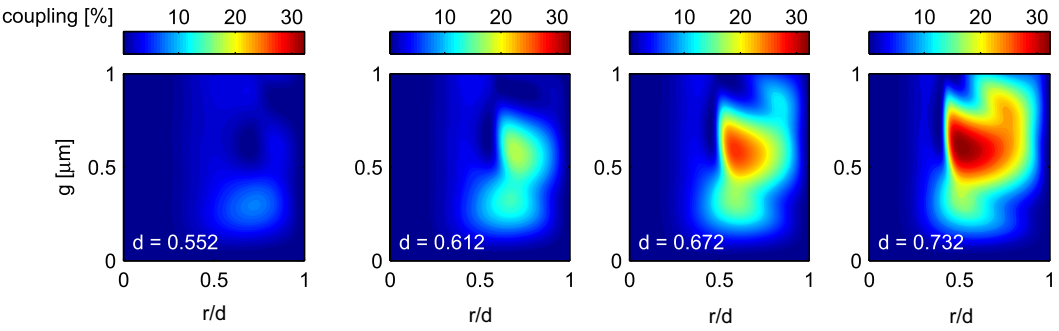

Figure 7.2: Coupling to the waveguide for each of the ±1 T rays (color-coded) versus groove depth g and fill factor r/d for TM illumination and selected values of d.

coupling obtained when g and r/d were varied according to Figure 7.2 versus grating period d for TM and TE polarization. Hence, for the purpose of a broadband reflection

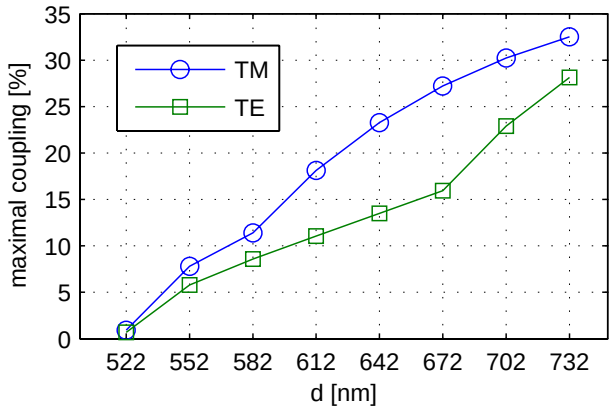

Figure 7.3: Maximum achievable coupling per diffraction order ± 1T for TM and TE polarization versus grating period d. For each point the groove depth was varied between 0 and 1 μm and the fill factor between 0 and 1.

peak large values for the grating period are favorable.

The direct connection between coupling and spectral width of the resonance is illustrated in Figure 7.4. The right-hand side of the Figure shows again the coupling to the waveguide versus groove depth and fill factor for a specific grating period. For three selected values of the groove depth (marked with three asterisks) and fixed fill

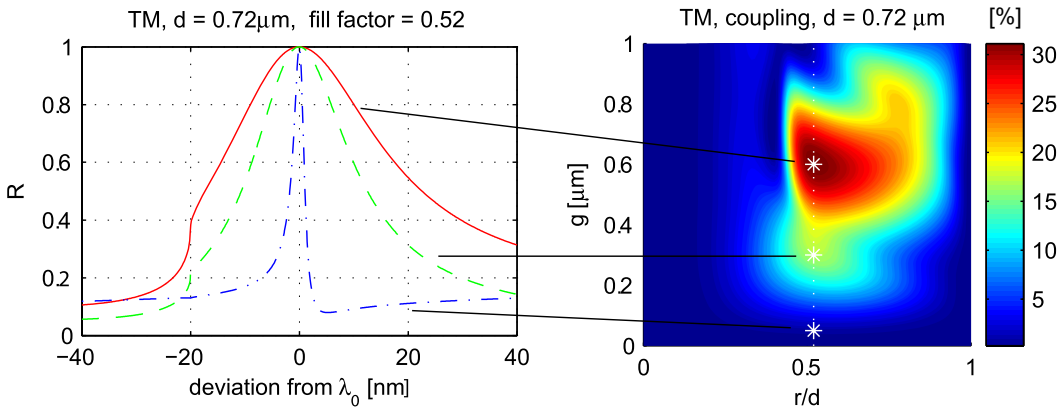

Figure 7.4: (right) TM coupling to the waveguide (color-coded) versus groove depth and fill factor. (left) Spectral response of three waveguide structures corresponding to the marked values in the right Figure. From a deviation of greater than -20 nm inequality (7.4) is no longer fulfilled which leads to the kinks in the curves.

factor, we determined the optimal waveguide thickness s_0 for a resonance peak around $\lambda_0 = 1064\,\text{nm}$. On the left hand side of Figure 7.4, we show the reflectivity versus the deviation from λ_0 for the corresponding waveguide coating.

We note that for materials with higher refractive index than $n_\text{H} = 2.04$ higher diffraction efficiencies (couplings to the waveguide) and therefore even broader reflection peaks are possible [7.13, 7.14].

7.4 Thickness of the coating

The crucial factor for coating thermal noise in gravitational wave detector test masses is the overall thickness of the high index coating material. To reach a reflectivity of $1 - R = 10\,\text{ppm}$ with a $\lambda/4$ stack of SiO_2 and Ta_2O_5, typically 40 layers are needed, adding up to $20\lambda/(4n_\text{H}) \approx 2.6\,\mu\text{m}$ overall tantala thickness. In contrast to this, a grating waveguide mirror can get along with a tantala thickness of much less than a wavelength.

In addition, if the total thickness of tantala in the waveguide structure is to be compared with a conventional mirror, one has to take into account that the grating region is not uniformly filled. Hence, to first-order approximation one can assume that

the coating thermal noise should be proportional to an effective tantala thickness of $s + g(r/d)$.

The layer thickness s determines the phase of the light travelling in the waveguide and hence the resonance condition of the device. The thickness s_0 for which a resonance occurs varies if the grating parameters g, r and d are changed as illustrated exemplary in Figure 7.5, where the power reflectivity is plotted versus the groove depth and the waveguide thickness. One can see a periodic behavior of the reflectivity as s varies as

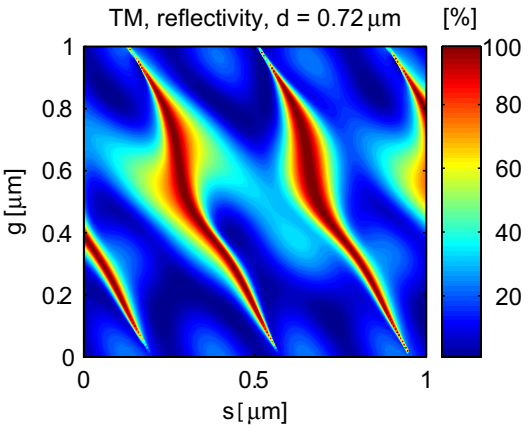

Figure 7.5: Color coded TM-reflectivity of a waveguide structure versus groove depth and waveguide thickness s. The values for $d, r/d$ and g correspond to the dotted line in Figure 7.4 (right). In this case 100 % reflectivity can be obtained for vanishing layer thickness at a groove depth of $g \approx 0.39\,\mu$m.

expected. More interesting to note is that for a certain value of g the 100 % reflectivity resonance occurs at $s = 0$. Accordingly the grating itself can provide perfect reflection and no waveguide layer is needed. This is extremely useful since the amount of the high index material can be greatly reduced. For vanishing waveguide layer thickness the explanation of the device via the ray picture presented in Figure 1 seems to break down. However, the results are based on a RCW analysis which is still valid for s=0

An optimal design of a grating waveguide coating for gravitational wave detectors will be a tradeoff between the broadest spectral response and the smallest effective tantala thickness. As an example we consider the GWS corresponding to the dashed (green) curve on the left hand side of Figure 7.4 which still has $\Delta\lambda_{\mathrm{FWHM}} \approx 22\,$nm.

With $g = 0.3\,\mu$m and $s \approx 0.06\,\mu$m the effective tantala thickness is only about $0.24\,\mu$m. This suggests a thermal noise reduction by more than an order of magnitude compared to a conventional coating.

7.5 Parameter tolerances

When designing diffractive structures one also has to consider how accurately grating parameters and layer thicknesses can be manufactured by state-of-the-art procedures and how strongly deviations from design values affect the performance of the waveguide coating. Here, we consider the fabrication errors in the waveguide thickness and how they can be compensated by tuning the laser wavelength. Figure 7.6 shows how the power reflectivity R of a waveguide is affected when the thickness of the waveguide or the wavelength of the laser deviate from their optimal values s_0 and λ_0, respectively. A

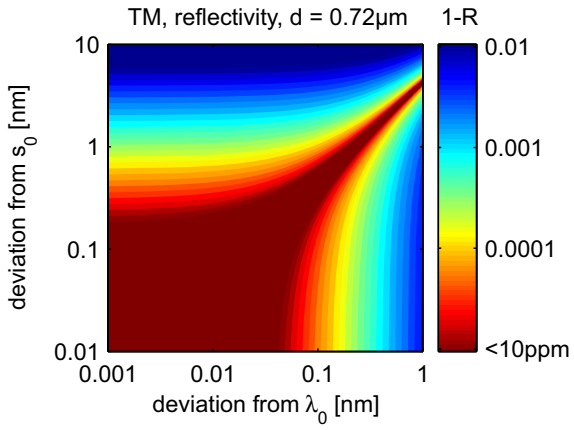

Figure 7.6: (Color-coded)Reflectivity plotted as 1-R versus the deviation from optimal wavelength λ_0 and deviation from optimal waveguide thickness $s_0 \approx 239\,$nm. Other parameters for the grating: $g = 0.6\,\mu$m; $r/d = 0.52$.

typical power reflectivity requirement for GW detectors is $(1 - R) < 10\,$ppm. Typical production accuracies of thin films are on the order of 1nm. The deviation from s_0 could be compensated by tuning the laser wavelength a small fraction of a nanometer. Deviations in other grating parameters affect the reflectivity by a similar way.

7.6 Conclusion

We have proposed a high reflectivity grating waveguide coating for advanced gravitational wave detectors which can provide perfect reflection despite the small amount of coating material that is needed. This has great potential to lower the coating thermal noise of high reflectivity mirrors. Focussing on a laser wavelength of $\lambda_0 = 1064\,\mathrm{nm}$ and tantala as the coating material we presented sample calculations of the spectral response of the coating as well as the overall tantala thickness of the coating. Our analysis was based on RCW analysis and assumed plane wave inputs as well as infinite gratings. Future theoretical work will include gaussian input beams and finite grating size effects. On top of that more sophisticated designs of grating waveguide structures like double periodic structures [7.15] or double gratings [7.16] will also be investigated. Future experimental work aims at fabrication and characterization of such devices as an alternative to conventional high reflectivity multilayer dielectric coating stacks. An important issue will be the reduction of optical loss that may arise from writing errors during grating fabrication.

Acknowledgements

This work has been supported by Deutsche Forschungsgemeinschaft within the Sonderforschungsbereich TR7. The authors would also like to thank T. Clausnitzer, E.-B. Kley and A. Tünnermann for fruitful discussions.

References

[7.1] V. B. Braginsky, M. L. Gorodetsky and S. P. Vyatchanin, *Thermodynamical fluctuations and photo-thermal shot noise in gravitational wave antennae,* Phys. Lett. A **264**, 1 (1999).

[7.2] G. M. Harry et al., *Thermal noise in interferometric gravitational wave detectors due to dielectric optical coatings,* Class. Quantum Grav. **19**, 897 (2002).

[7.3] M. M. Fejer et al., *Thermoelastic dissipation in inhomogeneous media: loss measurements and displacement noise in coated test masses for interferometric gravitational wave detectors,* Phys. Rev. D **70**, 082003 (2004).

[7.4] `www.ligo.caltech.edu/advLIGO`

[7.5] J. Agresti, G. Castaldi, R. DeSalvo, V. Galdi, V. Pierro, and I. M. Pinto, *Optimized multilayer dielectric mirror coatings for gravitational wave interferometers,* Proc. SPIE **6286**, 628608 (2006).

[7.6] G. M. Harry et al., *Thermal noise from optical coatings in gravitational wave detectors,* Appl. Opt. **45**, 1569 (2006).

[7.7] V. B. Braginsky, and S. P. Vyatchanin, *Corner reflectors and quantum-nondemolition measurements in gravitational wave antennae,* Phys. Lett. A **324**, 345 (2004).

[7.8] A. Sharon, D. Rosenblatt, A. A. Friesem, *Resonant grating waveguide structures for visible and near-infrared radiation,* J. Opt. Soc. Am. A **14**, 2985 (1997).

[7.9] A. Sharon, D. Rosenblatt, and A. A. Friesem, *Narrow spectral bandwidths with grating waveguide structures,* Appl. Phys. Lett. **69**, 4154 (1996).

[7.10] A. Sharon, D. Rosenblatt, A. A. Friesem, H. G. Weber, H. Engel, and R. Steingrueber, *Light modulation with resonant grating-waveguide structures,* Opt. Lett. **21**, 1564 (1996).

[7.11] D. Rosenblatt, A. Sharon, A. A. Friesem, *Resonant grating waveguide structures,* IEEE J. Quantum Electron. **33**, 2038 (1997).

[7.12] M. G. Moharam, and T. K. Gaylord, *Diffraction analysis of dielectric surface-relief gratings,* J. Opt. Soc. Am. **72**, 1385 (1982).

[7.13] C. F. R. Mateus, M. C. Y. Huang, D. Yunfei, A. R. Neureuther, C. J. Chang-Hasnain, *Ultrabroadband mirror using low-index cladded subwavelength grating,* IEEE Photon. Technol. Lett. **16**, 518 (2004).

[7.14] C. F. R. Mateus, M. C. Y. Huang, Lu Chen, C. J. Chang-Hasnain, Y. Suzuki, *Broad-band mirror (1.12-1.62 μm) using a subwavelength grating,* IEEE Photon. Technol. Lett. **16**, 1676 (2004).

[7.15] F. Lemarchand, A. Sentenac, H. Giovannini, *Increasing the angular tolerance of resonant grating filters with doubly periodic structures,* Opt. Lett. **23**, 1149 (1998).

[7.16] C. Kappel, A. Selle, M. A. Bader, and G. Marowsky, *Resonant double-grating waveguide structures as inverted Fabry-Perot interferometers,* J. Opt. Soc. Am. B **21**, 1127 (2004).

Chapter 8

Summary

8.1 Conclusion

The purpose of the work described here was the investigation of grating applications for high precision interferometers, especially for those in gravitational wave detection. Because the design and fabrication of adequate gratings for such interferometric applications constitutes its own field of research, the investigation was carried out by two groups. Within one joint project of a Transregional Collaborative Research Center (SFB/TR7 of the Deutsche Forschungsgemeinschaft), a group of the Institut für Angewandte Physik in Jena researched and developed custom-designed gratings, while our group in Hannover used the gratings to develop laser interferometric concepts. Results of the latter, which include the exploration of two grating resonator concepts as well as a high reflectivity coating concept on the basis of a grating waveguide structure, were reported in this thesis.

The all-reflective resonator concept based on a grating in first order Littrow mount has analog features to its conventional transmissive counterpart. The concept had already been demonstrated and was understood. However, its compatibility with low optical loss requirements was in question, because it needed gratings with high diffraction efficiency which were thought to have high scattering losses. It was experimentally shown that present grating production technology already allows for high (99.635 %) diffraction efficiency gratings with an overall optical loss of less than 0.2 % and that

cavities built thereof can reach a finesse of greater than 1500.

The main focus of the thesis lay in the investigation of three-port coupled linear Fabry-Perot cavities, where a grating in second order Littrow mount serves as a coupler. This somewhat more complex configuration had not been investigated before and hence, basic questions had to be solved. Successful experimental demonstrations of the configuration as well as thorough theoretical analyses of its features were presented. The key point to understanding the input-output relations of such cavities was an analysis of the phase relations for a generic three-port device. Fundamental principles such as energy conservation and reciprocity, rather than properties of a physical realization of the grating, led to a formulation of phase relations which is valid for all three-port gratings. Interestingly, this analysis not only led to a clarification of phase relations between the three ports governing the interferometric properties of the cavity, but moreover, it led to a deeper understanding of diffraction gratings themselves. Specifically, it revealed fundamental constraints for diffraction efficiencies of certain orders. Only with the knowledge of the phase relations as well as the constraints for diffraction efficiencies, is a proper design of three-port coupled cavities and their couplers possible.

In both all-reflective cavity concepts presented, a grating structure in combination with a high reflectivity coating acts as beam splitter adding one or two extra light paths to the specular reflected light. The third concept presented in this thesis also employs a grating structure to diffract an incoming beam into two additional orders. But instead of reflected orders, it employs transmitted diffraction orders to couple light into a thin waveguide. In a simplified model such grating waveguide structures can also be understood as inverted Fabry-Perot cavities. Using this model, it was shown how to optimize parameters by means of Rigorous Coupled Wave analysis to obtain a grating waveguide coating with broad spectral response and small overall thickness which can act as a high reflectivity but low thermal noise coating.

8.2 Outlook

The combination of two different research fields in one project, namely microstructure technology (Jena) and laser interferometry (Hannover), has mutually stimulated

both. The Hannover group clearly benefited from the production of gratings which allowed for the construction of new interferometer topologies. They led, for example, to further theoretical investigations of general new features such as three-port coupled interferometry. On the other hand, the Jena group, for example, profited from our interferometric measurements, because they revealed precise information about the optical loss and the maximally reached diffraction efficiency of the gratings, which are valuable information for the optimization of their design and production process. Hence, it is intended to extend this fruitful collaboration.

The next steps towards grating interferometers within gravitational wave detection will be taken. A further reduction of optical loss due to scattering is one important topic. Since a reduction of scattering cannot be achieved by means of polishing, other techniques have to be considered. One approach is to apply the coating on top of the grating structure instead of placing the coating beneath it. A comparative study within our project [8.1, 8.2] showed a considerable reduction of scattering for this case. Independent from the position of the coating, scattering will have to be reduced further by more accurately shaped grating patterns showing more uniformity over the whole grating area. This will be achieved by improved microstructure technology for optical component fabrication.

Due to the many applications of diffraction gratings – or more generally, of diffractive optical elements – in other areas of science and industry, research and development concerning their production technologies will most likely expand further. Since the introduction of dielectric diffraction gratings in the 90s of last century, their quality has steadily increased, as is indicated by the increase of the maximal diffraction efficiency reported in published journal articles (see Figure 8.1).

It is easy to envisage that future gravitational wave detectors will profit in a similar manner from semiconductor industry, which pushes microstructure technology, as current detectors have profited from the coating technology [8.7] pushed by the gyroscope and telecommunication sector several years ago.

Promising is the installation of an adapted version of a semiconductor Lithography system [8.8] by the Jena group in 2006. This machine allows for more accurately shaped groove pattern leading to improved optical properties of gratings [8.9]. Moreover, it is capable of scaling the gratings up to a size of 30 cm diameter, which is sufficiently

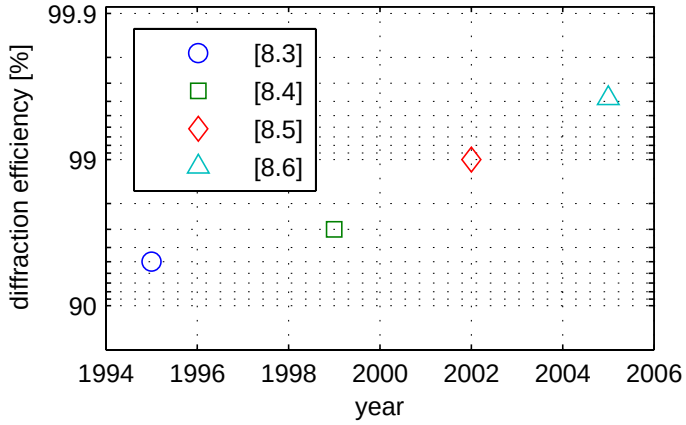

Figure 8.1: Development of maximally achieved diffraction efficiency for dielectric gratings over recent years. To the authors knowledge, the values shown represent record values at the time of publication. Reference [8.6] is Chapter 2 of this thesis.

large for advanced interferometer test masses. However, holographic generation (by means of interference lithography) of large grating pattern instead of direct writing using ion beams has also shown to be capable of providing large gratings in good quality [8.10, 8.11], and should be considered as an alternative production process for the gratings to be used in gravitational wave detectors.

Besides the availability of gratings with adequate size and quality, some other particularities have to be considered when gratings are used in interferometers. The following four features will affect the design and possibly the performance of grating interferometers, and will therefore be the subject of further study.

Wavelength dependence of diffraction angles: The diffraction angles of all non-zero orders which are used to split beams, depend on the wavelength of the laser light. Hence, interferometer alignment will not only have to account for appropriate positions of the optical elements but also the adequate laser wavelength. In addition, carrier- and sideband light fields will not share exactly the same optical path because of their frequency difference.

Asymmetric beam shaping: Due to different diffraction angles, the beam propagation for the various diffraction orders generally differs [8.12]. Thus, an asymmetry is introduced which affects the interferometer design. Consider, for example, a Michelson

interferometer with a four-port grating as a central beam splitter (Figure 1.1). The initial round beam will stay round in the arm formed from specular reflection but will become elliptical in that of the first diffraction order. Generally, good spatial overlap of the two beams after propagating differently in the arms will not be given, and has to be specially accounted for in the design of the interferometer [8.13].

Susceptibility to roll movements: Usually the test masses in gravitational wave detectors show cylindrical symmetry, therefore their roll movement is of no concern. Gratings are merely invariant for translational displacement in direction parallel to the grating grooves, but certainly not for rotation. Therefore roll movement can be considered an additional degree of freedom which needs to be investigated.

Susceptibility to transverse movement: Translational displacement of a flat mirror parallel to its surface will generally not cause a phase shift to the light reflected from it. However, it has been noted that a translational displacement of a grating parallel to its surface in a direction perpendicular to the grating grooves *will* induce a phase shift [8.14]. It has to be clarified to what extent this phase shift affects grating interferometers.

We intend to study the above mentioned issues experimentally, and theoretically by means of interferometer simulations. The recent success of experiments has already stimulated other research groups to study aspect of grating interferometry. A group at the University of Birmingham is working on extending a standard interferometer simulation program to include grating beam splitters, see Appendix B. Our GEO600 colleagues at the University of Glasgow plan to install a fully suspended 10 m-cavity based on the three-port coupler concept introduced here [8.15]. Moreover, a group in Stanford University reactivates its grating research effort in collaboration with San Jose State University [8.16].

Further research will also be directed towards the general potential of multi-port interferometry with gratings. One useful application of a three-port coupled cavity has already been identified, namely for frequency stabilization of lasers [8.17].

References

[8.1] T. Clausnitzer, E.-B. Kley, A. Tünnermann, A. Bunkowski, O. Burmeister, K. Danzmann, R. Schnabel, S. Gliech, A. Duparré, *Ultra low-loss low-efficiency diffraction gratings,* Opt. Express **13**, 4370 (2005).

[8.2] T. Clausnitzer, E.-B. Kley, A. Tünnermann, A. Bunkowski, O. Burmeister, K. Danzmann, R. Schnabel, A. Duparré, S. Gliech, *Low-loss gratings for next-generation gravitational wave detectors,* in: M. L. Fulton, J. D. Kruschwitz (eds.) Advances in Thin-Film Coatings for Optical Applications II, Proc. SPIE **5870**, 153 (2005).

[8.3] M. D. Perry, R. D. Boyd, J. A. Britten, D. Decker, B. W. Shore, C. Shannon, and E. Shults, *High-efficiency multilayer dielectric diffraction gratings,* Opt. Lett. **20**, 940 (1995).

[8.4] K. Hehl, J. Bischoff, U, Mohaupt, M. Palme, and B. Schnabel, *High-efficiency dielectric reflection gratings: design, fabrication, and analysis,* Appl. Opt. **38**, 6257 (1999).

[8.5] J. A. Britten, S. J. Bryan, L. J. Summers, H. T. Nguyen, B. W. Shore, O. Lyngnes, *Large aperture, high-efficiency multilayer dielectric reflection gratings,* Opt. Soc. America. **2**, CPDB7-1, Washington (2002).

[8.6] A. Bunkowski, O. Burmeister, T. Clausnitzer, E.-B. Kley, A. Tünnermann, K. Danzmann, R. Schnabel, *Optical characterization of ultrahigh diffraction efficiency gratings,* Appl. Opt. **45**, 5795 (2006).

[8.7] N. A. Robertson, *Laser interferometric gravitational wave detectors,* Class. Quantum Grav. **17**, R19 (2000).

[8.8] Electron Beam Lithography System Vistec SB350 OS, Vistec Electron Beam GmbH.
`http://www.vistec-semi.com/`

[8.9] E.-B. Kley, *personal communication.*

[8.10] P. T. Konkala, *Design and analysis of a scanning beam interference lithography system for patterning gratings with nanometer-level distortions,* Ph.D. thesis, Massachusetts Institute of Technology (2003).

[8.11] J. A. Britten et al., *Advanced dielectric grating technology for high-energy petawatt lasers,* Quantum Electronics and Laser Science Conference **3**, 2035 (2005).

[8.12] A. E. Siegman, *ABCD-matrix elements for a curved diffraction grating,* J. Opt. Soc. Am. A **2**, 1793 (1985).

[8.13] D. Friedrich, *Michelson Interferometer mit diffraktivem Strahlteiler,* Diplomarbeit, Universität Hannover (2006).

[8.14] S. Wise, V. Quetschke, A. J. Deshpande, G. Mueller, D. H. Reitze, D. B. Tanner, B. F. Whiting, Y. Chen, A. Tünnermann, E. Kley, and T. Clausnitzer *Phase Effects in the Diffraction of Light: Beyond the Grating Equation,* Phys. Rev. Lett. **95**, 013901 (2005).

[8.15] M. Plissi, *personal communication.*

[8.16] P. Beyersdorf, *personal communication.*

[8.17] R. Schnabel, O. Burmeister, A. Bunkowski, A. Thüring, R. Rinkleff, and K. Danzmann, *Laser Device,* International patent application, PCT/EP 2006/062626 (2006).

Appendix A

Diffraction efficiency calculations

As mentioned in Section 1.3.1 the grating Equation (1.1), merely predicts the number and orientation of diffraction orders for a given grating but not the power distribution among them. To obtain it one has to solve the corresponding Maxwell equations with appropriate boundary conditions which account for the characteristics of the radiation source as well as for the discontinuities of the electromagnetic field at the interfaces of the grating.

If the grating structures are large compared to the wavelength ($d \gg \lambda$), simplified scalar approximations like the Kirchhoff-type simulations are usually appropriate to analyze the properties of the grating. For $d \ll \lambda$ the grating can be modelled as a homogeneous effective medium which eases the computation of diffraction efficiencies.

However, the gratings discussed in this work have $d \sim \lambda$, a regime where exact theories need to be used, which requires more computational effort. Several different exact (also called rigorous or accurate) methods have been developed, please see References [A.1, A.2] for an overview. Some of the methods have been implemented in commercially available programs. For the grating simulations presented in Chapter 7, UNIGIT [A.3], a program employing the method of Rigorous Coupled Wave Analysis and the Rayleigh Fourier Method [A.4–A.7], was used. We chose the program, because it had been widely used and tested by the group of our project partners in Jena.

To conduct efficiency calculations the user can open a GUI, where the physical properties of the grating (including the coating) can be defined, as well as information

about the light source (wavelength, polarization, angle of incidence) can be given. In addition, the accuracy of the calculation, which is given by the number of Rayleigh orders to be included in the calculation, can be defined. The user can choose a start and end value for a single parameter which is to be varied linearly. Once the calculation has finished, the phase shift or diffraction efficiency for the various orders can be plotted versus the parameter varied.

This method works well but becomes extremely cumbersome, if recursive searches for certain grating properties are to be conducted, which involve the variation of several parameters. Hence the author developed MATLAB scripts to automate searches in multidimensional parameter spaces and store the results in arrays which can readily be used by MATLAB for visualization.

References

[A.1] M. Nevière and E. Popov, *Grating Electromagnetic Theory User Guide,* Journal of Imaging Science and Technology **41**, 315 (1997).

[A.2] `http://www.pcgrate.com/etestlab/calculat`

[A.3] `http://www.unigit.com`

[A.4] L. Li, *Use of Fourier series in the analysis of discontinuous periodic structures,* J. Opt. Soc. Am. A **13**, 1870 (1996).

[A.5] L. Li, *Formulation and comparison of two recursive matrix algorithms for modeling layered diffraction gratings,* J. Opt. Soc. Am. A **13**, 1024 (1996).

[A.6] L. Li, *New formulation of the Fourier modal method for crossed surface-relief gratings,* J. Opt. Soc. Am. A **14**, 2758 (1997).

[A.7] L. Li, *Note on the S-matrix propagation algorithm,* J. Opt. Soc. Am. A **20**, 655 (2003).

Appendix B

An extension of FINESSE to include gratings

Interferometer simulations provide valuable information during the design and commissioning of laser interferometric gravitational wave detectors. To handle the complexity of the models that describe advanced interferometers configurations with multiple cavities, several programs have been developed which automate the computational task of interferometer analysis. Many of these programs have been made available to the gravitational wave community [B.1].

For optical simulations FINESSE [B.2] is a widely used program. The user can build any kind of virtual interferometer using standard optical components. FINESSE allows for a fast computation of the light field amplitudes at every point in the interferometer by translating the interferometer description into a set of linear equations and solving it numerically.

There are many useful applications for the program. They include computation of modulation-demodulation error signals, transfer functions, and shot noise limited sensitivities as well as effects of mode matching and misalignments and many others. Due to its versatility FINESSE has become an important tool not only for experimentalists working on large scale laser interferometers as well as on their prototypes, but also for theorists who, for example, asses new interferometric setups for improved sensitivity.

When diffraction gratings are used as beam splitters in interferometers, novel fea-

tures emerge and simulations can be very useful to understand them. However, the components that could be used in FINESSE only included standard optics, but no diffraction gratings. Hence the author developed his own MATLAB scripts to simulate certain aspects of grating aided interferometers. Such scripts work well for simple simulations, but are only of limited utility, because firstly, they become hard to use when the complexity of the interferometer grows, and secondly, they do not include the many features that a mature interferometer simulation program provides. Hence, it was desirable to extend the functionality of FINESSE by including diffraction gratings as accepted optical elements.

Andreas Freise had developed FINESSE during the work towards his Ph.D. thesis [B.3] at the GEO600 detector in Hannover. Working then at the VIRGO detector and currently at the University of Birmingham, he has consecutively developed the program to improve its performance, and was happy to collaborate with the author to add grating features.

To do so, we had to define what kind of gratings would be considered, how they would be treated in the program, and what grating features were important to the computations. Every component used in FINESSE has a characteristic number of n nodes, corresponding to the possible input and outputs. Mirrors (defined as an optical surface for normal incidence), lenses as well as the component *space* have two nodes, and a beam splitter (defined as a mirror for oblique incidence) has four nodes. A $n \times n$ matrix is used to describe the local coupling of an element with the input and output fields. Hence, the coupling of light fields can be described by either a 2×2 or a 4×4 matrix, although the latter has several zero entries because only pairwise coupling of two ports is present.

In principle, when using gratings, n can be any number greater than one, if incidence angle, wavelength, and grating period are chosen accordingly, see the grating equation (1.1). Hence, a definition of a universal grating component in FINESSE would not be useful, because it would not have a characteristic n. Therefore, it was decided to define different grating components according to the number of ports they form. Three different grating components, with two, three, and four ports respectively, were defined.

The description of two and four port gratings were straightforward, because they are

analogous to mirror and beam splitter components. The coefficients for the amplitude transmission and reflection, which describe mirrors, only have to be replaced with these for zeroth and first order diffraction for the grating.

The description of a three-port grating (we restricted ourselves to the symmetric case as discussed in Chapter 4) is more complex and follows the matrix of Equation (4.7). In this case all three ports couple and the phase relation between the ports is not fixed as is the case for the two- and four-port grating. The according phases can be written as functions of the diffraction coefficients for the various orders, see Equations (4.10)–(4.12).

The use of a grating component in the extended version of FINESSE is simple. One has to choose the number of ports, a grating period, and the values for the various diffraction orders. In the case of first-order and second-order Littrow mount (corresponding to two-port and three-port gratings respectively) the corresponding Littrow angles are calculated automatically. In the case of the four-port grating (a non-Littrow configuration) an incident angle can be chosen and the angle of the first diffraction order is calculated.

The angle of incidence and the diffraction angles are relevant if one is interested in the beam shape of the laser light. In this case FINESSE performs the analysis using Hermite-Gauss modes instead of simple plane waves, for which a propagating beam is described by its Gaussian beam parameter, that is transformed according to the well-known ABCD matrix-formalism [B.4]. Every component, including propagation through free space, has its own characteristic ABCD-matrix. To account for diffraction of Gaussian beams at gratings, the not so well known ABCD matrix for a diffraction grating [B.5] had to be implemented. In the simplified case of a plane grating it reads

$$\begin{pmatrix} A & B \\ C & D \end{pmatrix} = \begin{pmatrix} \cos\beta_m/\cos\alpha & 0 \\ 0 & \cos\alpha/\cos\beta_m \end{pmatrix} \tag{B.1}$$

for the tangential plane when the notation of Equation (1.1) is used. For the sagittal plane the appropriate matrix is just the unity matrix, because the Gaussian beam will not be affected in this direction.

The introduced extension of FINESSE is particularly useful in exploring complex interferometer configurations which include three-port coupled cavities because it includes their coupling matrix. Moreover, it is useful to analyze the effect of *asymmetric*

beam shaping in grating interferometers, as outlined in Chapter 8. The other three issues described in Chapter 8 cannot yet be easily addressed with the current extension, but further addition of grating features is planned.

For more information on the notation and usage of the novel components, please see the manual of a new version (> 0.99) of FINESSE, by Andreas Freise, who actually implemented the features.

References

[B.1] `http://www.phys.ufl.edu/LIGO/LIGO/STAIC.html`

[B.2] `http://www.rzg.mpg.de/~adf/`

[B.3] A. Freise, *The Next Generation of Interferometry: Multi-Frequency Optcal Modelling, Control Concepts and Implementation,* Ph.D. thesis, Universität Hannover (2003).

[B.4] A. E. Siegman, *Lasers*, University Science Books, Sausalito (1986).

[B.5] A. E. Siegman, *ABCD-matrix elements for a curved diffraction grating,* J. Opt. Soc. Am. A **2**, 1793 (1985).

Appendix C

About the author

Publications within the grating project

[C.1] A. Bunkowksi, O. Burmeister, P. Beyersdorf, K. Danzmann, R. Schnabel, T. Clausnitzer, E.-B. Kley, and A. Tünnermann, *Low-loss grating for coupling to a high-finesse cavity,* Opt. Lett. **29**, 2342 (2004).

[C.2] A. Bunkowski, O. Burmeister, K. Danzmann, and R. Schnabel, *Input-output relations for a three-port grating coupled Fabry-Perot cavity,* Opt. Lett. **30**, 1183 (2005).

[C.3] T. Clausnitzer, E.-B. Kley, A. Tünnermann, A. Bunkowski, O. Burmeister, K. Danzmann, R. Schnabel, A. Duparré, S. Gliech, *Low-loss gratings for next-generation gravitational wave detectors,* in: M. L. Fulton, J. D. Kruschwitz (eds.) Advances in Thin-Film Coatings for Optical Applications II, Proc. SPIE **5870**, 153 (2005).

[C.4] T. Clausnitzer, E.-B. Kley, A. Tünnermann, A. Bunkowski, O. Burmeister, K. Danzmann, R. Schnabel, S. Gliech, A. Duparré, *Ultra low-loss low-efficiency diffraction gratings*, Opt. Express **13**, 4370 (2005).

[C.5] R. Schnabel, A. Bunkowski, O. Burmeister, and K. Danzmann, *Three-port beam splitters-combiners for interferometer applications,* Opt. Lett. **31**, 658 (2006).

[C.6] A. Bunkowski, O. Burmeister, K. Danzmann, R. Schnabel, T. Clausnitzer, E.-B. Kley, A. Tünnermann, *Demonstration of three-port grating phase relations,* Opt. Lett. **31**, 2384 (2006).

[C.7] A. Bunkowski, O. Burmeister, T. Clausnitzer, E.-B. Kley, A. Tünnermann, K. Danzmann, R. Schnabel, *Diffractive Optics for Gravitational Wave Detectors,* J. Phys.: Conf. Ser. **32**, 333 (2006).

[C.8] A. Bunkowski, O. Burmeister, T. Clausnitzer, E.-B. Kley, A. Tünnermann, K. Danzmann, R. Schnabel, *Optical characterization of ultrahigh diffraction efficiency gratings,* Appl. Opt. **45**, 5795 (2006).

[C.9] R. Schnabel, O. Burmeister, A. Bunkowski, A. Thüring, R. Rinkleff, and K. Danzmann, *Laser Device,* International patent application, PCT/EP 2006/062626 (2006).

[C.10] A. Bunkowski, O. Burmeister, D. Friedrich, R. Schnabel, and K. Danzmann, *High reflectivity grating waveguide coatings for 1064 nm,* Class. Quantum Grav. **23**, 7297 (2006).

[C.11] A. Bunkowski, *All-reflective interferometry with nano-structured optics,* (published as a research highlight article in the Biannual Report 2004/2005 of the Max-Planck-Institut für Gravitationsphysik, available at `www.aei.mpg`).

Publications within the GEO and LIGO projects

[C.12] J. R. Smith et al., *Commissioning, characterization and operation of the dual-recycled GEO 600,* Class. Quantum Grav. **21**, S1737 (2004).

[C.13] B. Abbott et al., *Limits on gravitational-wave emission from selected pulsars using LIGO data,* Phys. Rev. Lett. **94**, 181103 (2005).

[C.14] H. Grote et al., *The status of GEO 600,* Class Quantum Grav. **22**, S193 (2005).

[C.15] B. Abbott et al., *Search for gravitational waves associated with the gamma ray burst GRB030329 using the LIGO detectors,* Phys. Rev. D **72**, 042002 (2005).

[C.16] B. Abbott et al., *Upper limits on gravitational wave bursts in LIGO's second science run,* Phys. Rev. D **72**, 062001 (2005).

[C.17] B. Abbott et al., *Search for gravitational waves from primordial black hole binary coalescences in the galactic halo,* Phys. Rev. D **72**, 082002 (2005).

[C.18] B. Abbott et al., *Search for gravitational waves from galactic and extra-galactic binary neutron stars,* Phys. Rev. D **72**, 082001 (2005).

[C.19] B. Abbott et al., *First all-sky upper limits from LIGO on the strength of periodic gravitational waves using the Hough transform,* Phys. Rev. D **72**, 102004 (2005).

[C.20] B. Abbott et al., *Upper limits from the LIGO and TAMA detectors on the rate of gravitational-wave bursts,* Phys. Rev. D **72**, 122004 (2005).

[C.21] B. Abbott et al., *Search for gravitational waves from binary black hole inspirals in LIGO data,* Phys. Rev. D **73**, 062001 (2006).

[C.22] B. Willke et al., *The GEO-HF project,* Class. Quantum Grav. **23**, S207 (2006).

[C.23] H. Lück et al., *Status of the GEO600 detector,* Class. Quantum Grav. **23** S71 (2006).

[C.24] B. Abbott et al., *Joint LIGO and TAMA300 search for gravitational waves from inspiralling neutron star binaries,* Phys. Rev. D **73**, 102002 (2006).

Curriculum vitae

Alexander Bunkowski

Davenstedter Str. 8
D-30449 Hannover
e-mail: albunk@aei.mpg.de

date of birth: 22.02.1976
place of birth: Kassel
nationality: German

08/03 – 12/06	Research associate within the Sonderforschungsbereich TR7, Institut für Gravitationsphysik, Universität Hannover and Max-Planck-Gesellschaft.
06/02 – 06/03	Diploma thesis, Institut für Quantenoptik, Universität Hannover.
03/2003	Experimental work, Laboratoire Kastler Brossel, Ecole Normale Supérieure, Paris, France.
02/01 – 07/03	Physics studies, Universität Hannover.
02/00 – 02/01	Physics studies, Australian National University, Canberra.
10/99 – 02/00	International Physics Programme, Universität Bonn.
10/97 – 09/99	Physics studies, Universität Hannover.
08/96 – 08/97	Civil service, Hannover.
05/1996	Abitur, Matthias-Claudius-Gymnasium Gehrden.
08/92 – 06/93	High school stay, Ohio and Utah, USA.